Article

Neuron

De Novo Mutation in Genes Regulating Neural Stem Cell Fate in Human Congenital Hydrocephalus

Highlights

- Exome sequencing identifies novel genetic drivers of congenital hydrocephalus (CH)
- *De novo* and inherited rare variants in four genes explain ~10% of CH cases
- All four CH genes (*TRIM71*, *SMARCC1*, *PTCH1*, and *SHH*) regulate neural stem cell fate
- These data implicate aberrant neurogenesis in the pathogenesis of a subset of CH

Authors

Charuta Gavankar Furey, Jungmin Choi, Sheng Chih Jin, ..., Murat Günel, Richard P. Lifton, Kristopher T. Kahle

Correspondence

kristopher.kahle@yale.edu

In Brief

Congenital hydrocephalus (CH) is a major cause of childhood morbidity and mortality, affecting 1 in 1,000 live births and representing up to 3% of all pediatric hospital charges. Using data from the largest CH exome sequencing study to date, Furey et al. identify four genes (*TRIM71*, *SMARCC1*, *PTCH1*, and *SHH*) not previously implicated in CH. Remarkably, all four genes regulate ventricular zone neural stem cell fate and, together, explain ~10% of CH cases. These findings implicate impaired neurogenesis in pathogenesis of a significant number of CH patients, with potential diagnostic, prognostic, and therapeutic ramifications.

Furey et al., 2018, Neuron *99*, 302–314
July 25, 2018
https://doi.org/10.1016/j.neuron.2018.06.019

CellPress

CellPress

Neuron
Article

De Novo Mutation in Genes Regulating Neural Stem Cell Fate in Human Congenital Hydrocephalus

Charuta Gavankar Furey,[1,2,19] Jungmin Choi,[1,19] Sheng Chih Jin,[1,20] Xue Zeng,[1,20] Andrew T. Timberlake,[1,20] Carol Nelson-Williams,[1] M. Shahid Mansuri,[2] Qiongshi Lu,[3] Daniel Duran,[2] Shreyas Panchagnula,[2] August Allocco,[2] Jason K. Karimy,[2] Arjun Khanna,[4] Jonathan R. Gaillard,[2] Tyrone DeSpenza,[2] Prince Antwi,[2] Erin Loring,[1] William E. Butler,[4] Edward R. Smith,[5] Benjamin C. Warf,[5] Jennifer M. Strahle,[6] David D. Limbrick,[6] Phillip B. Storm,[7,8] Gregory Heuer,[7,8] Eric M. Jackson,[9] Bermans J. Iskandar,[10] James M. Johnston,[11] Irina Tikhonova,[12] Christopher Castaldi,[12] Francesc López-Giráldez,[12] Robert D. Bjornson,[12] James R. Knight,[1,12] Kaya Bilguvar,[12] Shrikant Mane,[12] Seth L. Alper,[13] Shozeb Haider,[14] Bulent Guclu,[15] Yasar Bayri,[16] Yener Sahin,[16] Michael L.J. Apuzzo,[2] Charles C. Duncan,[2] Michael L. DiLuna,[2] Murat Günel,[1,2] Richard P. Lifton,[1,17,21] and Kristopher T. Kahle[1,2,18,21,22,*]

[1]Department of Genetics, Yale University School of Medicine, New Haven, CT 06510, USA
[2]Department of Neurosurgery, Yale University School of Medicine, New Haven, CT 06510, USA
[3]Department of Biostatistics & Medical Informatics, University of Wisconsin, Madison, WI 53706, USA
[4]Department of Neurosurgery, Massachusetts General Hospital, Harvard Medical School, Boston, MA 02114, USA
[5]Department of Neurosurgery, Boston Children's Hospital, Harvard Medical School, Boston, MA 02115, USA
[6]Department of Neurological Surgery and Pediatrics, Washington University in St. Louis School of Medicine, St. Louis, MO 63110, USA
[7]Department of Neurosurgery, Hospital of the University of Pennsylvania, Philadelphia, PA 19104, USA
[8]Division of Neurosurgery, Children's Hospital of Philadelphia, Philadelphia, PA, 19104, USA
[9]Department of Neurosurgery, Johns Hopkins School of Medicine, Baltimore, MD 21287, USA
[10]Department of Neurological Surgery, University of Wisconsin Medical School, Madison, WI 53726, USA
[11]Department of Neurosurgery, University of Alabama School of Medicine, Birmingham, AL 35233, USA
[12]Yale Center for Genome Analysis, Yale University, New Haven, CT 06510, USA
[13]Division of Nephrology and Center for Vascular Biology Research, Beth Israel Deaconess Medical Center, Department of Medicine, Harvard Medical School, Boston, MA 02215, USA
[14]Department of Pharmaceutical and Biological Chemistry, University College London School of Pharmacy, London WC1N 1AX, UK
[15]Kartal Dr. Lutfi Kirdar Research and Training Hospital, Istanbul 34860, Turkey
[16]Acibadem Mehmet Ali Aydinlar University, School of Medicine, Department of Neurosurgery, Division of Pediatric Neurosurgery, Istanbul 34752, Turkey
[17]Laboratory of Human Genetics and Genomics, The Rockefeller University, New York, NY 10065, USA
[18]Department of Cellular & Molecular Physiology, Yale University School of Medicine, New Haven, CT 06510, USA
[19]These authors contributed equally
[20]These authors contributed equally
[21]Senior author
[22]Lead Contact
*Correspondence: kristopher.kahle@yale.edu
https://doi.org/10.1016/j.neuron.2018.06.019

SUMMARY

Congenital hydrocephalus (CH), featuring markedly enlarged brain ventricles, is thought to arise from failed cerebrospinal fluid (CSF) homeostasis and is treated with lifelong surgical CSF shunting with substantial morbidity. CH pathogenesis is poorly understood. Exome sequencing of 125 CH trios and 52 additional probands identified three genes with significant burden of rare damaging *de novo* or transmitted mutations: *TRIM71* ($p = 2.15 \times 10^{-7}$), *SMARCC1* ($p = 8.15 \times 10^{-10}$), and *PTCH1* ($p = 1.06 \times 10^{-6}$). Additionally, two *de novo* duplications were identified at the *SHH* locus, encoding the PTCH1 ligand ($p = 1.2 \times 10^{-4}$). Together, these probands account for ~10% of studied cases. Strikingly, all four genes are required for neural tube development and regulate ventricular zone neural stem cell fate. These results implicate impaired neurogenesis (rather than active CSF accumulation) in the pathogenesis of a subset of CH patients, with potential diagnostic, prognostic, and therapeutic ramifications.

INTRODUCTION

Hydrocephalus has been defined as the active, progressive distension of the cerebral ventricular system resulting from inadequate passage of cerebrospinal fluid (CSF) from its point of production to its point of absorption (Rekate, 2008). This mechanism is evident in secondary hydrocephalus associated with brain tumors, infection, or hemorrhage, in which intracranial pressure is often elevated (Kahle et al., 2016). However, when infantile

hydrocephalus occurs without a known antecedent, it is classified as primary or congenital hydrocephalus (CH) (Tully and Dobyns, 2014). CH can occur in the absence of obstruction to CSF flow (communicating hydrocephalus) or with complete/partial intraventricular obstruction (non-communicating hydrocephalus), most often due to aqueductal stenosis. Cases of communicating CH with normal or low intracranial pressure (Bret and Chazal, 1995; Tully and Dobyns, 2014) raise the question of whether the development of ventriculomegaly is a primary active process or a secondary passive process.

CH is a major cause of childhood morbidity and mortality, affecting 1 in 1,000 live births (Munch et al., 2012; Simon et al., 2008) and costing the U.S. health care system alone $2 billion annually (Shannon et al., 2011; Simon et al., 2008). Current therapy consists of catheter-based CSF shunting and endoscopic approaches, surgeries with high rates of failure and morbidity (Kahle et al., 2016). Significant gaps in our understanding of the molecular pathophysiology of CH impede the development of preventive, diagnostic, and therapeutic measures (McAllister et al., 2015).

Few bona fide human CH-causing genes have been identified (Kousi and Katsanis, 2016). These include *L1CAM* mutation in X-linked hydrocephalus and aqueductal stenosis (OMIM# 307000; Rosenthal et al., 1992), which constitutes up to 3% of CH, and rare recessive mutations in *MPDZ* (OMIM# 603785; Al-Dosari et al., 2013), *CCDC88C* (OMIM# 236600; Ekici et al., 2010), *EML1*, and *WDR81* (Shaheen et al., 2017). These genes affect multiple cellular processes, confounding efforts to formulate a uniform paradigm of CH pathophysiology (Kousi and Katsanis, 2016). While ~40% of all CH cases are predicted to have a genetic etiology (Zhang et al., 2006), mutations in currently identified genes account for less than 5% of primary CH cases (Adle-Biassette et al., 2013; Haverkamp et al., 1999).

The sporadic nature of most CH cases limits the utility of traditional genetic approaches. This has motivated whole-exome sequencing (WES) of large patient cohorts, searching for genes mutated in affected subjects more often than expected by chance. This approach has proven powerful in other neurodevelopmental disorders (Deciphering Developmental Disorders Study, 2015, 2017), including brain malformations (Barak et al., 2011; Bilgüvar et al., 2010), epilepsy (Allen et al., 2013), craniosynostosis (Timberlake et al., 2016, 2017), autism (Awadalla et al., 2010; O'Roak et al., 2011; Neale et al., 2012; Sanders et al., 2012; Krumm et al., 2015), and others. We hypothesized that the apparent sporadic occurrence of CH may reflect, in some cases, damaging *de novo* mutations and/or transmitted mutations with incomplete penetrance.

RESULTS

Cohort Characteristics and Whole-Exome Sequencing

We recruited 177 probands with non-*L1CAM*-mutated CH in which hydrocephalus was the predominant phenotypic feature (see STAR Methods). All probands had undergone surgery for CSF diversion. The cohort included 125 parent-offspring sporadic CH trios, 47 singleton cases, and 5 multiplex kindreds (see STAR Methods; Table S1). 88 probands had communicating hydrocephalus and 89 had aqueductal stenosis. All study protocols were approved by the Yale Human Research Protection Program (HRPP) Institutional Review Board.

DNA was isolated, and WES was performed (Timberlake et al., 2016). 95.9% of targeted bases had 8 or more independent reads, and 92.7% had 15 or more (Table S2; Figure S1). 1,789 control trios that comprised unaffected siblings from the Simons simplex autism cohort were sequenced on the same platform and analyzed in parallel (Krumm et al., 2015). Variants were called using the Genome Analysis Toolkit (GATK) Haplotype Caller (McKenna et al., 2010; Van der Auwera et al., 2013), and allele frequencies were annotated in the Exome Aggregation Consortium (ExAC) and gnomAD databases (Lek et al., 2016; see STAR Methods). TrioDeNovo was used to identify *de novo* mutations, and MetaSVM was used to infer the impact of missense mutations (Dong et al., 2015). Direct Sanger sequencing of PCR amplicons containing the mutation verified variants in genes of interest.

We identified mutations in known CH genes in four probands, including one proband with compound heterozygous mutations in *MPDZ*, the cause of autosomal recessive (AR) non-syndromic hydrocephalus type 2 (OMIM# 615219; Al-Dosari et al., 2013); two male probands with transmitted D-mis mutations in *FLNA*, the cause of X-linked dominant (XLD) periventricular heterotopia (OMIM# 300049; Kamuro and Tenokuchi, 1993; Sheen et al., 2004); and one proband with compound heterozygous mutation in *CRB2* (Hydro122), the cause of a AR ventriculomegaly with cystic kidney disease (OMIM# 219730; Slavotinek et al., 2015).

Global Analysis of Burden of *De Novo* Mutation

We determined a *de novo* mutation rate of 1.4×10^{-8} per base pair, with 1.09 *de novo* coding region mutations per proband (Table 1), consistent with expectation and previous work (Homsy et al., 2015; Timberlake et al., 2017; Ware et al., 2015). The burden of *de novo* mutations in the control cohort was similar (Table S3; Figure S2).

We compared the observed and expected number of *de novo* mutations in all genes and among genes in the top quartile of brain expression at embryonic day 9.5 (E9.5; see STAR Methods). Protein-altering *de novo* mutations were significantly enriched over expectation in the latter group, contributing to an estimated 8% of cases (Table 1). Controls showed no enrichment of *de novo* mutations in any gene class (Table S3).

Five genes contained two or more protein-altering *de novo* mutations: *TRIM71*, *SMARCC1*, *PTCH1*, *PLOD2*, and *SGSM3* (Table S4). The first three genes have a probability of loss-of-function (LOF) intolerance (pLI) score $\geq$ 0.99; the latter two genes have pLIs of zero (Lek et al., 2016). The probability of finding five genes with two or more protein-altering *de novo* mutations in a cohort this size by chance is very low ($p = 1.1 \times 10^{-4}$). Four of these genes were in the upper quartile of expression in the developing brain. The probability of finding two or more protein-altering *de novo* mutations in four such genes in our cohort is very low ($p = 1.1 \times 10^{-4}$; Table S5).

Recurrent *De Novo* and Transmitted Mutations in *TRIM71*

LIN41/TRIM71, encoding lineage variant 41 (LIN41)/tripartite motif 71 ("TRIM71") (Reinhart et al., 2000; Slack et al., 2000),

Table 1. Observed and Expected *De Novo* Mutation Rates in 125 Probands with Congenital Hydrocephalus and CH Cases with Aqueductal Stenosis for Variant Classes by Phenotype and High Brain Expression

	Observed		Expected			
	n	Rate	n	Rate	Enrichment	p
Hydro (125)						
All	137	1.10	139.7	1.12	0.98	0.60
Synonymous	32	0.26	39.7	0.32	0.81	0.91
Missense	89	0.71	87.8	0.70	1.01	0.46
D-Mis	16	0.13	16.5	0.13	0.97	0.58
LOF	16	0.13	12.3	0.10	1.30	0.18
Protein-Altering	105	0.84	100.0	0.80	1.05	0.32
Damaging	32	0.26	28.7	0.23	1.11	0.30
Hydro (125) – High Brain Expressed						
All	48	0.38	36.9	0.30	1.30	0.04[a]
Synonymous	12	0.10	10.3	0.08	1.16	0.34
Missense	30	0.24	23.2	0.19	1.29	0.10
D-Mis	5	0.04	4.4	0.04	1.14	0.45
LOF	6	0.05	3.4	0.03	1.78	0.13
Protein-Altering	36	0.29	26.5	0.21	1.36	0.04[a]
Damaging	11	0.09	7.8	0.06	1.42	0.16
Hydro + AS (66)						
All	78	1.18	73.8	1.12	1.06	0.33
Synonymous	22	0.33	20.9	0.32	1.05	0.44
Missense	47	0.71	46.3	0.70	1.01	0.48
D-Mis	12	0.18	8.7	0.13	1.38	0.17
LOF	9	0.14	6.5	0.10	1.39	0.21
Protein-Altering	56	0.85	52.8	0.80	1.06	0.35
Damaging	21	0.32	15.2	0.23	1.38	0.09
Hydro + AS (66) – High Brain Expressed						
All	30	0.45	19.5	0.30	1.54	0.01[a]
Synonymous	9	0.14	5.5	0.08	1.65	0.10
Missense	17	0.26	12.2	0.19	1.39	0.11
D-Mis	4	0.06	2.3	0.04	1.72	0.21
LOF	4	0.06	1.8	0.03	2.25	0.11
Protein-Altering	21	0.32	14.0	0.21	1.50	0.04[a]
Damaging	8	0.12	4.1	0.06	1.95	0.05[a]

n, the number of *de novo* mutations; Rate, the number of *de novo* mutations per individual; Enrichment, ratio of observed to expected number of mutations; Hydro, congenital hydrocephalus; High Brain Expression, top quartile of expression; AS, aqueductal stenosis; Missense, tolerated missense mutations as predicted by MetaSVM; D-Mis, damaging missense mutations as predicted by MetaSVM; LOF, loss of function denotes premature termination, frameshift, or splice site mutations; Damaging, D-miss and LOF mutations.
[a]p value $\leq$ 0.05

harbored three novel *de novo* mutations, including the identical heterozygous *de novo* p.Arg608His mutation in two unrelated probands with prenatally diagnosed communicating hydrocephalus (Hydro101-1 and Hydro102-1) (Figure 1; Table S6). During the course of this study, Hydro102-1 became pregnant and transmitted the p.Arg608His mutation to her son, who was prenatally diagnosed with communicating hydrocephalus (Figure 1; Figure S5). A third *de novo TRIM71* mutation (p.Arg796His) was identified in Hydro100-1, who had prenatally diagnosed communicating CH (Hydro100-1). All CH patients harboring *TRIM71* mutations underwent surgical CSF shunting at birth because of extreme ventriculomegaly. The probability of finding three or more protein-altering *de novo* mutations in *TRIM71* by chance in a cohort of this size is 2.15×10^{-7}, surpassing genome-wide significance (Table 2) (Ware et al., 2015). *TRIM71* is highly intolerant to LOF mutation (pLI = 0.99) and missense variation (*Z* score = 5.69) (Lek et al., 2016). With 105 protein-altering *de novo* missense mutations in our cohort, the probability of seeing any instances of the identical mutation at any position in the coding region by chance is very remote ($p = 5.24 \times 10^{-4}$).

TRIM71 is the homolog of *C. elegans Lin-41*, a target of the let-7 (lethal 7) microRNA (miRNA) in the heterochronic pathway that regulates stem cell fate (Ecsedi and Grosshans, 2013). TRIM71, like Lin-41, mediates post-transcriptional silencing of mRNAs via direct interactions of its NHL domain and the 5′ or 3′ UTRs of target genes (Aeschimann et al., 2017; Ecsedi and Grosshans, 2013; Slack and Ruvkun, 1998; Vella et al., 2004). TRIM71 also contains ubiquitin ligase activity conferred by its RING domain (Nguyen et al., 2017). The NHL domain in TRIM71 consists of six repeats, each 40–50 residues long, that jointly comprise a barrel-like six-bladed β-propeller (Loedige et al., 2015). The *de novo* p.Arg608His and p.Arg796His mutations are at homologous positions in different blades of NHL domains. Arginines at these positions are conserved among orthologs from *H. sapiens* to *C. elegans* and reside in RPQGV motifs (Figure 1). The NHL domain of TRIM71 is the closest homolog of the NHL domain of *D. melanogaster* Brat (Loedige et al., 2013, 2014), which has been co-crystallized bound to a target RNA (Loedige et al., 2015). In this structure, the amino groups of side chains of the mutated arginines form hydrogen bonds with either the phosphate backbone (p.Arg796) or a uracil base (p.Arg608) of target RNA (Figure 1; Figure S3). These interactions are predicted to be altered by histidine substitution. While these mutations were predicted as tolerated by MetaSVM, they are predicted as damaging by 43 of 45 other predicting algorithms, including the very conservative MPC-D algorithm (see STAR Methods; Samocha et al., 2017). The recurrence of the identical *de novo* mutation and the fact that the third *de novo* mutation occurs at a homologous position in a different NHL domain suggest that *TRIM71* mutations may not be simple LOF mutations.

In situ hybridization in E12.5 mouse brain (Figure 1; Figure S4) revealed abundant Trim71 expression in the neuroepithelium and ventricular zone (Cuevas et al., 2015; Maller Schulman et al., 2008). Analogous to its heterochronic expression in *C. elegans* (Kanamoto et al., 2006; Slack et al., 2000), Trim71 expression significantly decreases during development (Figure 1) (Schulman et al., 2005; Yu et al., 2010). Trim71 is highly expressed in neural progenitor cells (NPCs) of early mouse embryos (until E11.5) but declines secondary to increased expression of let-7 and mir-125 miRNAs as neural differentiation proceeds (Chen et al., 2012; Schulman et al., 2005). *Trim71* deletion in mice results in exencephaly and embryonic lethality (failure of closure of the cephalic end of the neural tube) by

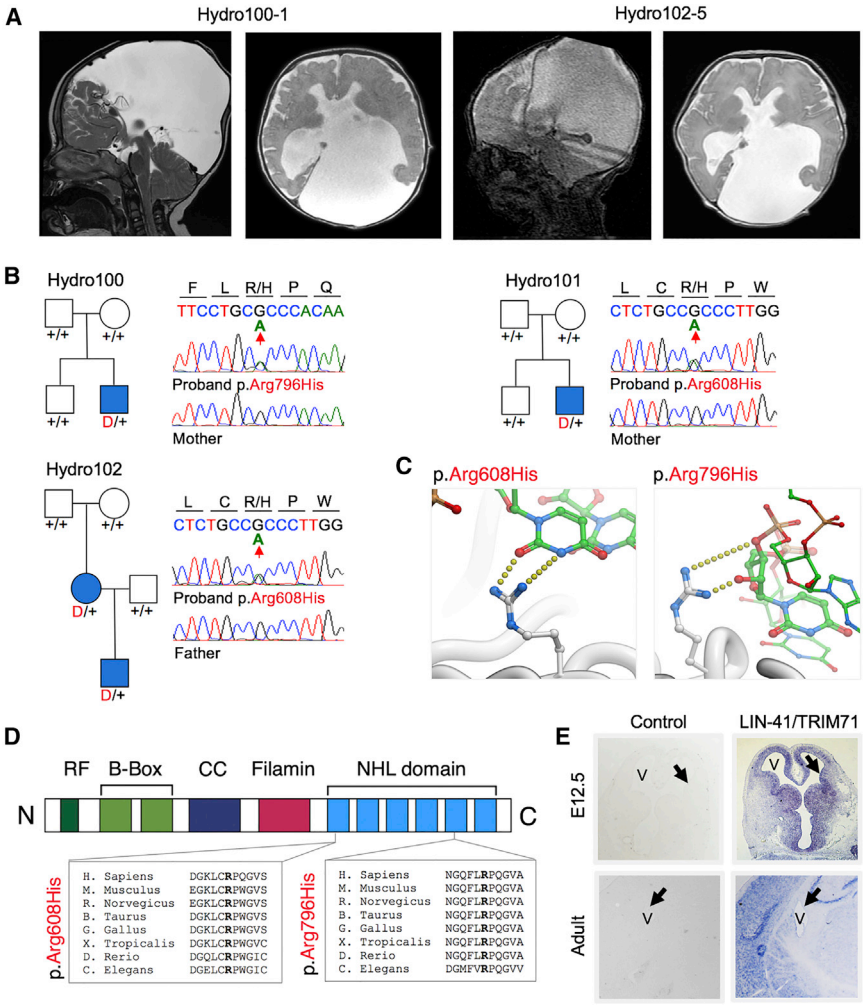

Figure 1. Recurrent, Identical *De Novo* Mutations in *LIN-41/TRIM71* Encoding the let-7 miRNA Target TRIM71

(A) Representative sagittal (left) and axial (right) brain magnetic resonance images of CH probands Hydro100-1 and Hydro102-5 show communicating hydrocephalus.

(B) Pedigrees with Sanger-verified mutated bases (red) and the corresponding wild-type bases marked on the chromatograms.

(C) Structural modeling of *TRIM71* mutation impact. The positively charged guanidinium side chain of p.Arg796 interacts with the negatively charged sugar-phosphate backbone of target RNAs to aid in maintaining the spatial position of the nucleic acid. Mutation of this p.Arg796 residue to the imidazole ring of histidine ($\Delta\Delta G = 2.0$ kcal/mol) is predicted to disrupt this interaction (right). The side chain of p.Arg608 makes hydrogen bonds with uracil in target RNAs. The p.Arg608His mutation ($\Delta\Delta G = 1.6$ kcal/mol) is predicted to disrupt these hydrogen bonds (left).

(D) Mapping of *TRIM71* mutations. p.Arg608His and p.Arg796His affect conserved residues in the 16th position of the respective 1st and 5th blades of TRIM71's NHL domain, which mediates the binding of target RNA.

(E) *In situ* hybridization of wild-type E12.5 and adult mouse brains for Trim71 showing signals in the ciliated neuroepithelium and ventricular zone (V, ventricle; arrow, neuroepithelium at E12.5 and ependymal layer in adulthood; 2.5× and 10× magnification).

E10 (Maller Schulman et al., 2008). Trim71 maintains NPC pluripotency NPCs by regulating the balance between self-renewal and differentiation via the post-transcriptional silencing of its target mRNAs (Chang et al., 2012; Ecsedi and Grosshans, 2013; Mitschka et al., 2015; Worringer et al., 2014). The neural tube closure defect in *Trim71* knockout mice results from decreased proliferation and precocious differentiation of NPCs (Chen et al., 2012).

Multiple *De Novo* and Transmitted Mutations in *SMARCC1*

Two novel, damaging *de novo* mutations were identified in *SMARCC1*, encoding BAF155, a 155-kD subunit of the BRG1/BRM-associated factor (BAF; *S. cerevisiae* SWI/SNF) chromatin remodeling complex (Wang et al., 1996). These mutations included a p.Lys891fs*4 mutation (in Hydro106-3) and a predicted damaging missense p.His526Pro mutation (in Hydro105-1) located in a conserved position in the SWIRM domain, which mediates BAF complex subunit interactions (Da et al., 2006) (Figure 2). p.His526Pro occurred in a proband with obstructive CH with aqueductal stenosis and no other affected family members. p.Lys891fs*4 was *de novo* in an unaffected father (Hydro106-3) of three children with prenatally diagnosed CH with aqueductal stenosis. Two of these offsprings died in utero from obstructive hydrocephalus, while the surviving child inherited p.Lys891fs*4. In this cohort, the probability of seeing two damaging *de novo* mutations in *SMARCC1* was 2.69×10^{-6} (Table 2).

Three additional, previously unidentified, transmitted LOF mutations in *SMARCC1* were found in three other CH probands with severe obstructive CH with aqueductal stenosis. In each of these kindreds, the proband was the sole affected member with mutation transmission from an unaffected parent (Figure 2; Figure S6; Table S7). The probability of two *de novo* damaging mutations and three rare transmitted LOFs occurring in *SMARCC1* in this cohort was 8.15×10^{-10}; this is a conservative estimate since *SMARCC1* is highly intolerant to LOF mutation (pLI of 1), with far fewer LOF mutations than expected (3 LOF *SMARCC1* mutations among 60,706 individuals in the ExAC database, and 2 among 3,578 autism controls).

In situ hybridization demonstrated that Smarcc1, like Trim71, is highly expressed in the neuroepithelium and ventricular zone but reduced in later brain development (Ho et al., 2009; Tuoc et al., 2013a; Yan et al., 2008) (Figure 2; Figure S4). *Smarcc1* knockout causes embryonic lethality in mice (Kim et al., 2001). Roughly 20% of *Smarcc1*$^{+/-}$ mice (Kim et al., 2001) and ~80% of mice homozygous for a missense allele (*Baf155*$^{msp/msp}$)

Table 2. Meta-analysis of Protein-Altering *De Novo* Mutations and Loss-of-Function Heterozygous Mutations in Probands for Genes with Multiple *De Novo* Mutations

	De Novo Mutations				Transmitted Loss-of-Function (LOF)						
Gene	# observed	# expected	enrichment	p value	# observed	# expected	enrichment	Binomial p value	Meta p value	pLI	High Brain Expression Rank
SMARCC1	2	2.3×10^{-3}	861.7	2.7×10^{-6}[a]	3	4.3×10^{-2}	70.5	1.2×10^{-5}	8.2×10^{-10}[a]	1.0	97.4
PTCH1	2	1.5×10^{-3}	1374.3	1.1×10^{-6}[a]	1	3.8×10^{-2}	26.1	3.8×10^{-2}	7.2×10^{-7}[a]	1.0	93.2
TRIM71	3	1.1×10^{-2}	274.8	2.2×10^{-7}[a]	0	2.5×10^{-2}	0	1	3.5×10^{-6}	1.0	74.6
PLOD2	2	3.5×10^{-3}	580.2	5.9×10^{-6}	0	7.8×10^{-2}	0	1	7.7×10^{-5}	0	82.8
SGSM3	2	8.6×10^{-3}	232.2	3.7×10^{-5}	0	6.9×10^{-2}	0	1	4.1×10^{-4}	0	67.4

Meta-analysis performed by combining the p values from protein-altering *de novo* mutations and LOF heterozygous mutations using the Fisher's method with 4 degrees of freedom.

[a]p values surpassing the Bonferroni multiple testing correction (2.6×10^{-6}, 0.05/18,989) for p values tabulated by either *de novo*, heterozygous, or meta-analysis. Of note, the denovolyzeR p value of damaging *SMARCC1* mutations was calculated using 126 case-parent trios given the sporadic de novo mutation occurs in the proband's father (Hydro106-3).

(Harmacek et al., 2014) exhibit exencephaly similar to that of *Trim71* knockout mice (Harmacek et al., 2014; Narayanan et al., 2015; Nguyen et al., 2016). The exencephaly phenotype has been attributed to inappropriate proliferation and increased apoptosis of NPCs in the neural tube (Harmacek et al., 2014; Kim et al., 2001). Neuronal specific knockout of *Smarca4*, encoding a Smarcc1 binding partner in the BAF complex, causes hydrocephalus and aqueductal stenosis (Cao and Wu, 2015). NPC-specific BAF complexes regulate the proliferation, differentiation, and survival of mouse NPCs via transcriptional regulation of genes critical for telencephalon development (Narayanan et al., 2015).

De Novo and Transmitted Mutations in *PTCH1*

Two previously unidentified *de novo* LOF mutations were identified in *PTCH1*, encoding the Sonic Hedgehog (SHH) receptor (Eggenschwiler and Anderson, 2007) Patched-1 (Figure 3). Heterozygous LOF *PTCH1* mutations have been previously implicated in Gorlin syndrome (OMIM# 109400), featuring basal cell carcinomas and mandibular tumors, along with variable expressivity of other skeletal and non-skeletal phenotypes (Hahn et al., 1996). *De novo PTCH1* mutations included a start-loss mutation (p.Met152fs*1) and a splice donor site mutation (c.1503+3T>C) in unrelated CH probands with aqueductal stenosis (Figure 3; Figure S7; Table S8). Both mutations were heterozygous and occurred in probands of uniplex CH kindreds. A transmitted frameshift mutation in *PTCH1* (p.Leu664fs*12) was also found in two brothers with CH (Figure 3; Figure S7; Table S8). This mutation was transmitted from a mother who did not have hydrocephalus but had been diagnosed with Gorlin syndrome on the basis of numerous basal cell carcinomas. The probability of seeing at least two damaging *de novo* mutations by chance in a cohort of this size is 1.06×10^{-6}, surpassing genome-wide significance (Table 2) (Ware et al., 2015).

Consistent with previous results (Eggenschwiler et al., 2001; Goodrich et al., 1996, 1997; Takahashi and Osumi, 2002), *in situ* hybridization showed Ptch1 expression in hindbrain neuroepithelium (Figure 3; Figure S4). *Ptch1* knockout in mice results in exencephaly, neural tube overgrowth, and lethality between E9.0 and E10.5 (Ellis et al., 2003; Goodrich et al., 1997; Milenkovic et al., 1999). A significant fraction of $Ptch1^{+/-}$ mice develop hydrocephalus in two different genetic backgrounds (Svärd et al., 2009; Wetmore et al., 2000), similar to the variable expressivity seen in one of the multiplex kindreds. Penetrance of hydrocephalus in these mice increases to 100% for the homozygous quaking viable mutation ($Ptch1^{+/-}$; $qk^{v/v}$) (Gavino and Richard, 2011). Primary cilia in neuroepithelial cells sense gradients of SHH via PTCH1 and transduce these signals to regulate NPC proliferation, differentiation, and fate specification (Palma et al., 2005; Palma and Ruiz i Altaba, 2004).

De Novo Mutations in *PLOD2*

Two heterozygous *de novo* D-mis mutations were identified in the highly brain expressed (HBE) gene *PLOD2* (Table S9). *PLOD2* did not surpass thresholds for genome-wide significance. *PLOD2* encodes a lysyl hydroxylase previously implicated in AR Bruck syndrome type 2 (OMIM# 609220), a variant of osteogenesis imperfecta (McPherson and Clemens, 1997). Further work will be required to assess the significance of these mutations in CH.

De Novo Mutations in Neural Tube Closure and Formation

Gene ontology (GO) pathway analysis identified our significant CH gene set to be highly enriched for genes involved in "neural tube closure and formation." We searched for additional *de novo* mutations in genes in this GO pathway (Table S10). We found a single *de novo* missense mutation in *CELSR2* (p.Arg2812Trp), encoding cadherin EGF LAG seven-pass G-type receptor 2, and a single *de novo* missense mutation in *LRP6* (p.Val1415Phe), encoding a co-receptor with frizzled proteins in the WNT signaling pathway. *Celsr2* and *Lrp6* are highly expressed in ciliated neuroepithelia and regulate neurogenesis, and knockout of each gene results in lethal hydrocephalus in mice (Allache et al., 2014; Cuevas et al., 2015; Gavino and Richard, 2011; Harmacek et al., 2014; Maller Schulman et al., 2008; Tissir et al., 2010).

De Novo Duplications at the *SHH* Locus

Using the XHMM algorithm (Fromer and Purcell, 2001), we identified seven putative *de novo* copy number variants (CNVs) (see STAR Methods). Six of these, including five duplications and one

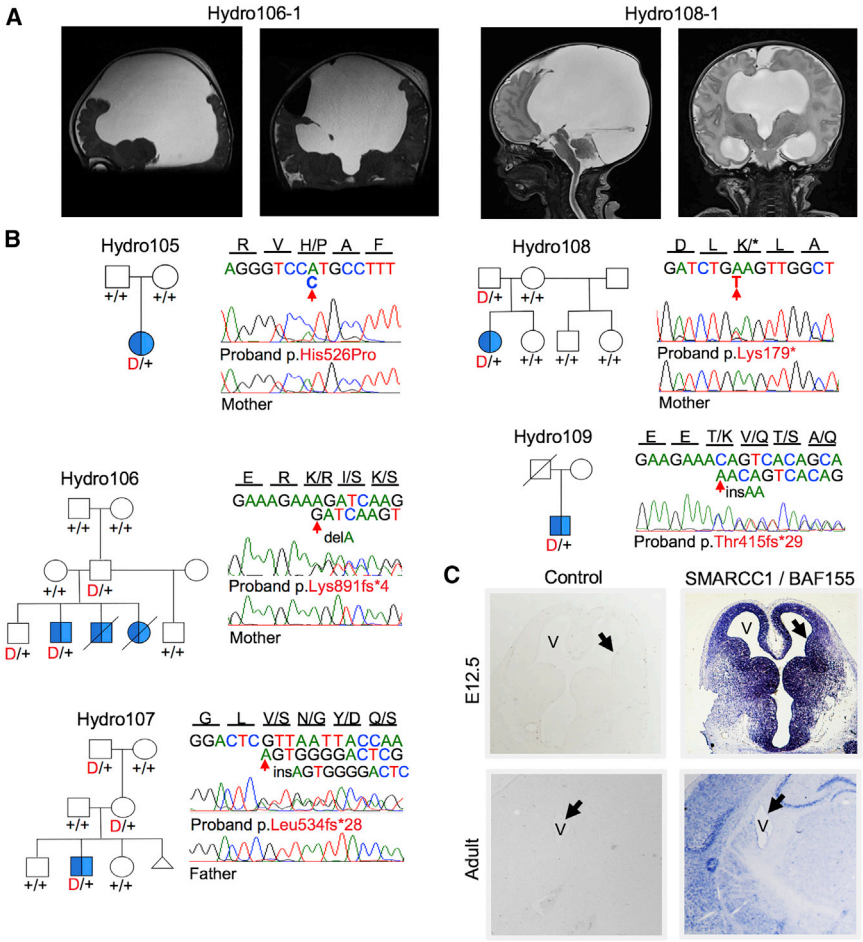

Figure 2. *De Novo* and Transmitted Mutations in *SMARCC1* Encoding the SWI/SNF Chromatin Modifier BAF155

(A) Representative sagittal (left) and coronal (right) brain magnetic resonance images of CH probands Hydro106-1 and Hydro108-1 with obstructive hydrocephalus.

(B) Pedigrees with Sanger-verified mutated bases and the corresponding normal alleles marked on the chromatograms.

(C) *In situ* hybridization of wild-type E12.5 and adult mouse brains for Smarcc1 showing signals in the ciliated neuroepithelium and ventricular zone (V, ventricle; arrow, neuroepithelium at E12.5, 2.5×, and ependymal layer in adulthood; 10× magnification).

deletion, were validated by independent tests (distortion of allelic ratios of heterozygous SNPs in implicated intervals or qPCR; Table S11). Two of these were duplications at the *SHH* locus, encoding SHH, the canonical ligand for PTCH1 that regulates neurogenesis by conferring positional information to ventral NPCs in the neural tube (Jessell and Sanes, 2000; Lupo et al., 2006). The probability of finding two duplications at the same locus among five duplication events with these gene compositions is very low ($p = 1.22 \times 10^{-4}$) (see STAR Methods).

DISCUSSION

Using exome sequencing, we implicate four new genes in human CH: *TRIM71*, *SMARCC1*, *PTCH1*, and *SHH* (Figure 4). High enrichment of mutations in these genes suggests their large effects on phenotypic risk. The genes showing heterozygous protein-altering *de novo* mutations are all highly intolerant to LOF mutation (pLI $\geq$ 0.99), and murine knockouts of each gene produce neural tube defects, including exencephaly (Feng et al., 2013; Gavino and Richard, 2011; Goodrich et al., 1997; Hahn et al., 1996; Harmacek et al., 2014; Maller Schulman et al., 2008). *SHH* encodes the PTCH1 ligand. *Ptch1*-deficient mice develop fatal hydrocephalus (Celen et al., 2017; Gavino and Richard, 2011). All four genes are expressed in the ciliated neuroepithelium and regulate NPC fate. Mutations in these four new genes account for 8.5% of cases; another 2.3% of cases are explained by previously identified genes.

From the inferred contribution of *de novo* point mutations to 8% of CH probands in our cohort and the number of genes with more than one *de novo* mutation, we estimate that additional genes contribute to CH by *de novo* point mutation (maximum likelihood estimate ~8 genes, with wide confidence interval) (Figures S8 and S9). This estimate is substantially smaller than autism and congenital heart disease (De Rubeis et al., 2014; Homsy et al., 2015; Iossifov et al., 2014; Sanders et al., 2012; Zaidi et al., 2013), consistent with the identification of multiple disease-causing genes from this relatively small cohort. Variants in non-coding elements of these genes might add to their contribution to CH. Sequencing of additional trios and isolated probands has high potential to detect additional rare mutations with large effect on disease risk.

All four cases of CH with *TRIM71* mutation had communicating hydrocephalus, whereas all five cases with *SMARCC1* mutation and all three cases with *PTCH1* mutation had aqueductal stenosis. From the prevalence of these two sub-phenotypes in our cohort (50.2% communicating versus 49.8% aqueductal, respectively) we calculate that this correlation was highly unlikely to occur by chance ($p = 0.002$). These observations support the pathogenicity of the mutations and suggest phenotypic subsets of CH are influenced by genetic determinants.

Our results suggest incomplete penetrance and variable expressivity of mutations in two CH genes. Four first-degree relatives of probands with the same mutation in *SMARCC1* and one relative of a *PTCH1* mutation proband had no evidence of hydrocephalus. Moreover, heterozygous LOF mutations in *PTCH1* are a well-described cause of Gorlin syndrome (Gorlin, 2004; Gorlin and Goltz, 1960), which can be associated with obstructive hydrocephalus due to medulloblastoma (Amlashi et al., 2003). Similar to murine hydrocephalus with

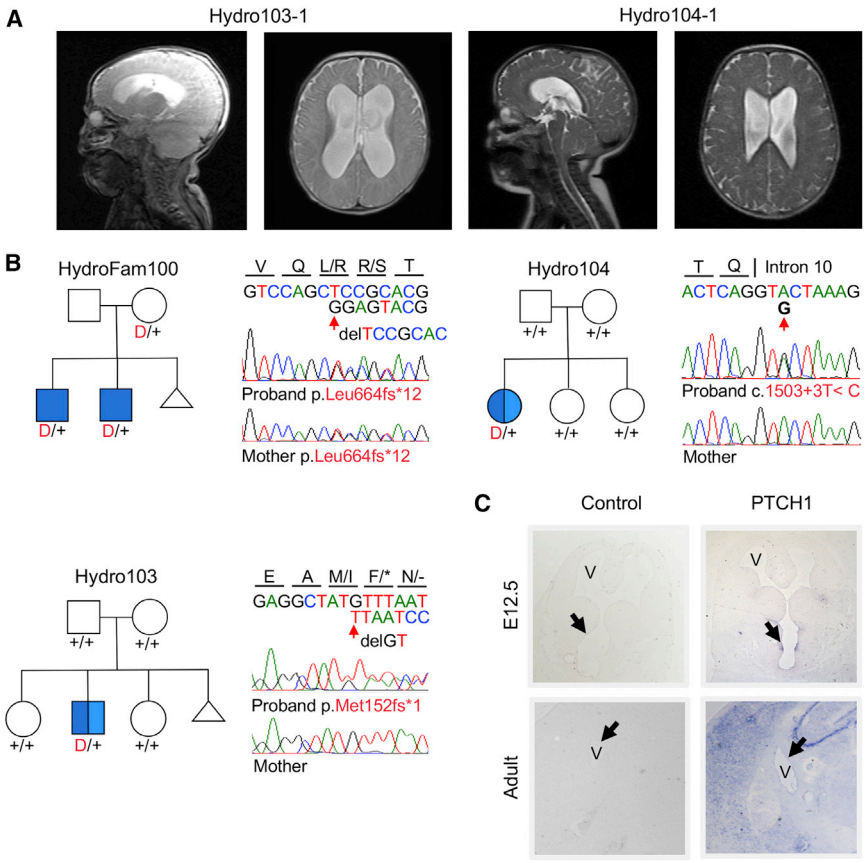

Figure 3. *De Novo* and Transmitted Mutations in *PTCH1* Encoding the Sonic Hedgehog Receptor Patched-1

(A) Representative sagittal (left) and axial (right) brain magnetic resonance images of CH probands Hydro103-1 and Hydro104-1 with obstructive hydrocephalus.

(B) Pedigrees with Sanger-verified mutated bases and the corresponding normal alleles marked on the chromatograms.

(C) *In situ* hybridization of wild-type E12.5 and adult mouse brains for Ptch1 demonstrates expression in the hindbrain neuroepithelium (V, ventricle; arrow, neuroepithelium at E12.5, 2.5×, and ependymal layer in adulthood; 10× magnification).

PTCH1 mutation (Wang et al., 2010a; Wetmore et al., 2015), our patients had hydrocephalus without CSF obstruction from medulloblastoma. In addition, a mutation-bearing parent of one of our probands had been diagnosed with Gorlin syndrome owing to numerous basal cell carcinomas but did not have hydrocephalus. This suggests that LOF mutations in our probands are functionally equivalent to those causing Gorlin syndrome and that these probands may be at risk of developing basal cell carcinomas. The determinants of incomplete penetrance and variable expressivity remain obscure but may be explained by common genetic (Timberlake et al., 2016) or environmental (Stuart et al., 2015) modifiers or by stochastic elements.

Similar to other Mendelian forms of CH (e.g., *L1CAM*) (Rosenthal et al., 1992), several CH patients harboring *TRIM71* and *SMARCC1* mutations exhibited other neurological findings and structural brain abnormalities in addition to hydrocephalus. All CH patients with *TRIM71* mutations and 3 of 5 CH patients with *SMARCC1* mutations exhibited neurodevelopmental delay and epilepsy. A mother and son with mutant *TRIM71* and ventriculomegaly had similar open schizencephalic clefts (Figure 1). Two patients with *SMARCC1* mutations exhibited schizencephalic clefts and possibly other structural brain abnormalities (Figure 2). These findings are consistent with TRIM71 and SMARCC1 regulating key aspects of brain development (Cuevas et al., 2015; Harmacek et al., 2014; Kim et al., 2001; Maller Schulman et al., 2008; Narayanan et al., 2015; Nguyen et al., 2016).

SMARCC1 and *PTCH1* in CH are LOF mutations. *TRIM71* exhibits a highly specific mutation spectrum involving either of two homologous arginines in the NHL domain that directly binds mRNAs (Chang et al., 2012; Loedige et al., 2013, 2014, 2015). While these mutations likely impair binding to normal target mRNAs, other gene functions, such as its putative ubiquitin ligase activity, may be preserved. Alternatively, these mutations could impart neomorphic effects that cause binding to new mRNAs. Similarly, the observed duplications of *SHH* suggest that these mutations are gain of function. Dosage loss of *PTCH1*, which inhibits downstream signaling via effect on the *SMO* receptor, and dosage gain of *SHH* would be similarly expected to increase downstream Hedgehog signaling (Briscoe and Thérond, 2013).

Ciliated neuroepithelial stem cells in the neural tube ventricular zone undergo proliferation accompanied by minimal differentiation during early embryogenesis. These cells become differentiated neurons (Ever and Gaiano, 2005; Merkle et al., 2004) in mice between E8 and E14 (Chen et al., 2006; Noctor et al., 2004), a transformation driven by significant alterations in gene expression (Yao et al., 2016). TRIM71, SMARCC1, and PTCH1 are all highly expressed in the ciliated neuroepithelium (Cuevas et al., 2015; Gavino and Richard, 2011; Tuoc et al., 2013b). SHH engages its receptor PTCH1 on neuroepithelial cilia. All five genes regulate the proliferation, fate specification, and/or differentiation of NPCs the development of the neural tube (Kim et al., 2001; Nguyen et al., 2017; Shikata et al., 2011).

The gene mutations reported here suggest the importance of *de novo* or transmitted mutations that alter the balance between NPC proliferation and differentiation in the pathogenic mechanism of CH. In support of this human genetic data, *Dusp16* deficiency in mice causes brain overgrowth and associated obstructive hydrocephalus due to hyperproliferation and expansion of ventricular zone NPCs at the level of the aqueduct (Zega et al., 2017). In contrast, the communicating hydrocephalus phenotype in a mouse model of the human ciliopathy Bardet-Biedl

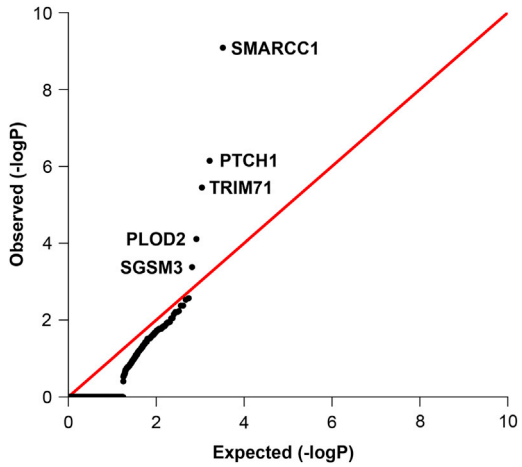

Figure 4. Meta-analysis of Rare *De Novo* and Transmitted Mutations in Mutation-Intolerant Genes

Quantile-quantile plot of observed versus expected p values from meta-analysis of protein-altering *de novo* and LOF transmitted heterozygous variants comparing the burden of rare variants in genes intolerant to LOF mutation (pLI $\geq$ 0.90, MAF $\leq 2 \times 10^{-5}$).

syndrome results from decreased proliferation and survival of NPCs (Carter et al., 2012). Interestingly, intraventricular hemorrhage in neonates, the most common cause of infantile secondary hydrocephalus (Mazzola et al., 2014; Robinson, 2012), is also associated with decreased NPC viability and associated cortical thinning (McAllister et al., 2017; Yung et al., 2011). A "neural stem cell" paradigm of hydrocephalus could provide a unifying mechanism to explain multiple forms of infantile hydrocephalus.

These findings have potential implications for CH treatment. Multiple non-neural mechanisms have been proposed to account for communicating hydrocephalus, including elevated venous pressure, arachnoid granulation immaturity, and lymphatic dysplasia (Govaert et al., 1991). However, given the new genetic data, a primary driver of some communicating forms of CH may not be attributable to active CSF accumulation and associated ventricular distension but rather impaired neurogenesis. In neonatal CH cases with normal or low intracranial pressure (Tully et al., 2016), it is unclear whether surgical CSF shunting addresses a pathologic feature of CH. Instead, it may expose CH patients to surgical morbidity without improving neurodevelopmental outcomes. The implications for families with CH children and their neurosurgeons will stimulate discussion and catalyze further investigation into CH pathogenesis and treatment.

STAR★METHODS

Detailed methods are provided in the online version of this paper and include the following:

- KEY RESOURCES TABLE
- CONTACT FOR REAGENT AND RESOURCE SHARING
- EXPERIMENTAL MODEL AND SUBJECT DETAILS
  - Subjects and Samples
  - Whole-Exome Sequencing and Variant Calling
- METHOD DETAILS
  - Kinship Analysis
  - Haplotype Phasing and Analysis of Inbreeding
  - Principal Component Analysis
  - *De Novo* and Inherited Variant Analysis and Filtering
  - Burden of *De Novo* Mutations
  - Contribution of *De Novo* Mutation to Congenital Hydrocephalus
  - Enrichment Analysis for the Dominant and Recessive Variants
  - Gene Ontology Enrichment Analysis
  - *In Silico* Splice-Site Prediction
  - Copy Number Variation Analysis
- QUANTIFICATION AND STATISTICAL ANALYSIS
  - *De Novo* CNV Permutation Test
  - Estimating the Number of Risk Genes
  - *In Situ* Hybridization
- DATA AND SOFTWARE AVAILABILITY

SUPPLEMENTAL INFORMATION

Supplemental Information includes nine figures and eleven tables and can be found with this article online at https://doi.org/10.1016/j.neuron.2018.06.019.

ACKNOWLEDGMENTS

We are grateful to the patients and families who participated in this research. We would also like to thank Jenna Koschnitzky, Amanda Garzón, and the entire Hydrocephalus Association (HA); Jeannine Rockefeller and Jeannette Votto (Yale); and Diego Morales (WashU). This work is supported by the Yale-NIH Center for Mendelian Genomics (5U54HG006504), NIH T32GM007205, NIH TL1 TR001864, Hydrocephalus Foundation, Howard Hughes Medical Institute, and Rudi Schulte Research Institute.

AUTHOR CONTRIBUTIONS

Conceptualization, C.G.F., R.P.L., and K.T.K.; Methodology, C.G.F., A.T.T., S.C.J., Q.L., R.P.L., and K.T.K.; Software, C.G.F., J.C., S.C.J., X.Z., A.T.T., and J.K.; Validation, C.G.F., J.C., S.C.J., X.Z., A.T.T., C.N.-W., and D.D.; Formal Analysis, C.G.F., S.C.J., and Q.L.; Investigations, C.G.F., A.T.T., C.N.-W., M.S.M., D.D., S.P., A.A., J.K.K., J.R.G., T.S., P.A., A.K., W.E.B., E.R.S., B.C.W., J.M.S., D.D.L., P.B.S., G.H., E.M.J., B.J.I., J.M.J., K.B., S.M., I.T., C.C., F.L.-G., J.K., S.L.A., S.H., B.G., Y.B., Y.S., M.L.J.A., C.C.D., M.L.D., M.G., R.P.L., and K.T.K.; Resources, C.N.-W., K.B., S.M., I.T., C.C., F.L.-G., R.D.B., J.K., S.L.A., M.G., R.P.L., and K.T.K.; Data Curation, C.G.F., J.C., S.C.J., X.Z., A.T.T., and J.K.; Writing – Original Draft, C.G.F., A.T.T., R.P.L., and K.T.K.; Writing – Reviewing & Editing, C.G.F., S.C.J., A.T.T., R.P.L., and K.T.K.; Visualization, C.G.F.; Supervision, R.P.L. and K.T.K.; Project Administration, C.G.F., C.N.-W., E.L., R.P.L., and K.T.K.; Funding Acquisition, R.P.L. and K.T.K.

DECLARATION OF INTERESTS

The authors declare no competing interests.

Received: February 13, 2018
Revised: April 3, 2018
Accepted: June 12, 2018
Published: July 5, 2018

REFERENCES

Adle-Biassette, H., Saugier-Veber, P., Fallet-Bianco, C., Delezoide, A.-L., Razavi, F., Drouot, N., Bazin, A., Beaufrère, A.-M., Bessières, B., Blesson,

S., et al. (2013). Neuropathological review of 138 cases genetically tested for X-linked hydrocephalus: evidence for closely related clinical entities of unknown molecular bases. Acta Neuropathol. *126*, 427–442.

Adzhubei, I.A., Schmidt, S., Peshkin, L., Ramensky, V.E., Gerasimova, A., Bork, P., Kondrashov, A.S., and Sunyaev, S.R. (2010). A method and server for predicting damaging missense mutations. Nat. Methods *7*, 248–249.

Aeschimann, F., Kumari, P., Bartake, H., Gaidatzis, D., Xu, L., Ciosk, R., and Großhans, H. (2017). LIN41 post-transcriptionally silences mRNAs by two distinct and position-dependent mechanisms. Mol. Cell *65*, 476–489.e4.

Al-Dosari, M.S., Al-Owain, M., Tulbah, M., Kurdi, W., Adly, N., Al-Hemidan, A., Masoodi, T.A., Albash, B., and Alkuraya, F.S. (2013). Mutation in MPDZ causes severe congenital hydrocephalus. J. Med. Genet. *50*, 54–58.

Allache, R., Lachance, S., Guyot, M.C., De Marco, P., Merello, E., Justice, M.J., Capra, V., and Kibar, Z. (2014). Novel mutations in Lrp6 orthologs in mouse and human neural tube defects affect a highly dosage-sensitive Wnt non-canonical planar cell polarity pathway. Hum. Mol. Genet. *23*, 1687–1699.

Allen, A.S., Berkovic, S.F., Cossette, P., Delanty, N., Dlugos, D., Eichler, E.E., Epstein, M.P., Glauser, T., Goldstein, D.B., Han, Y., et al.; Epi4K Consortium; Epilepsy Phenome/Genome Project (2013). De novo mutations in epileptic encephalopathies. Nature *501*, 217–221.

Amlashi, S.F., Riffaud, L., Brassier, G., and Morandi, X. (2003). Nevoid basal cell carcinoma syndrome: relation with desmoplastic medulloblastoma in infancy. A population-based study and review of the literature. Cancer *98*, 618–624.

Auton, A., Brooks, L.D., Durbin, R.M., Garrison, E.P., Kang, H.M., Korbel, J.O., Marchini, J.L., McCarthy, S., McVean, G.A., and Abecasis, G.R.; 1000 Genomes Project Consortium (2015). A global reference for human genetic variation. Nature *526*, 68–74.

Awadalla, P., Gauthier, J., Myers, R.A., Casals, F., Hamdan, F.F., Griffing, A.R., Côté, M., Henrion, E., Spiegelman, D., Tarabeux, J., et al. (2010). Direct measure of the de novo mutation rate in autism and schizophrenia cohorts. Am. J. Hum. Genet. *87*, 316–324.

Barak, T., Kwan, K.Y., Louvi, A., Demirbilek, V., Saygı, S., Tüysüz, B., Choi, M., Boyacı, H., Doerschner, K., Zhu, Y., et al. (2011). Recessive LAMC3 mutations cause malformations of occipital cortical development. Nat. Genet. *43*, 590–594.

Bilgüvar, K., Oztürk, A.K., Louvi, A., Kwan, K.Y., Choi, M., Tatli, B., Yalnizoğlu, D., Tüysüz, B., Cağlayan, A.O., Gökben, S., et al. (2010). Whole-exome sequencing identifies recessive WDR62 mutations in severe brain malformations. Nature *467*, 207–210.

Bret, P., and Chazal, J. (1995). Chronic ("normal pressure") hydrocephalus in childhood and adolescence. A review of 16 cases and reappraisal of the syndrome. Childs Nerv. Syst. *11*, 687–691.

Briscoe, J., and Thérond, P.P. (2013). The mechanisms of Hedgehog signalling and its roles in development and disease. Nat. Rev. Mol. Cell Biol. *14*, 416–429.

Browning, S.R., and Browning, B.L. (2007). Rapid and accurate haplotype phasing and missing-data inference for whole-genome association studies by use of localized haplotype clustering. Am. J. Hum. Genet. *81*, 1084–1097.

Cao, M., and Wu, J.I. (2015). Camk2a-Cre-mediated conditional deletion of chromatin remodeler Brg1 causes perinatal hydrocephalus. Neurosci. Lett. *597*, 71–76.

Carter, C.S., Vogel, T.W., Zhang, Q., Seo, S., Swiderski, R.E., Moninger, T.O., Cassell, M.D., Thedens, D.R., Keppler-Noreuil, K.M., Nopoulos, P., et al. (2012). Abnormal development of NG2+PDGFR-α+ neural progenitor cells leads to neonatal hydrocephalus in a ciliopathy mouse model. Nat. Med. *18*, 1797–1804.

Carter, H., Douville, C., Stenson, P.D., Cooper, D.N., and Karchin, R. (2013). Identifying Mendelian disease genes with the variant effect scoring tool. BMC Genomics *14* (*Suppl 3*), S3.

Celen, C., Chuang, J.C., Luo, X., Nijem, N., Walker, A.K., Chen, F., Zhang, S., Chung, A.S., Nguyen, L.H., Nassour, I., et al. (2017). *Arid1b* haploinsufficient mice reveal neuropsychiatric phenotypes and reversible causes of growth impairment. eLife *6*, 6.

Chang, H.M., Martinez, N.J., Thornton, J.E., Hagan, J.P., Nguyen, K.D., and Gregory, R.I. (2012). Trim71 cooperates with microRNAs to repress Cdkn1a expression and promote embryonic stem cell proliferation. Nat. Commun. *3*, 923.

Chen, C.P., Lin, S.P., Wang, T.H., Chen, Y.J., Chen, M., and Wang, W. (2006). Perinatal findings and molecular cytogenetic analyses of de novo interstitial deletion of 9q (9q22.3–>q31.3) associated with Gorlin syndrome. Prenat. Diagn. *26*, 725–729.

Chen, J., Lai, F., and Niswander, L. (2012). The ubiquitin ligase mLin41 temporally promotes neural progenitor cell maintenance through FGF signaling. Genes Dev. *26*, 803–815.

Choi, Y., Sims, G.E., Murphy, S., Miller, J.R., and Chan, A.P. (2012). Predicting the functional effect of amino acid substitutions and indels. PLoS ONE *7*, e46688.

Chun, S., and Fay, J.C. (2009). Identification of deleterious mutations within three human genomes. Genome Res. *19*, 1553–1561.

Cromer, M.K., Starker, L.F., Choi, M., Udelsman, R., Nelson-Williams, C., Lifton, R.P., and Carling, T. (2012). Identification of somatic mutations in parathyroid tumors using whole-exome sequencing. J. Clin. Endocrinol. Metab. *97*, E1774–E1781.

Cuevas, E., Rybak-Wolf, A., Rohde, A.M., Nguyen, D.T.T., and Wulczyn, F.G. (2015). Lin41/Trim71 is essential for mouse development and specifically expressed in postnatal ependymal cells of the brain. Front. Cell Dev. Biol. *3*, 20.

Da, G., Lenkart, J., Zhao, K., Shiekhattar, R., Cairns, B.R., and Marmorstein, R. (2006). Structure and function of the SWIRM domain, a conserved protein module found in chromatin regulatory complexes. Proc. Natl. Acad. Sci. USA *103*, 2057–2062.

Davydov, E.V., Goode, D.L., Sirota, M., Cooper, G.M., Sidow, A., and Batzoglou, S. (2010). Identifying a high fraction of the human genome to be under selective constraint using GERP++. PLoS Comput. Biol. *6*, e1001025.

De Rubeis, S., He, X., Goldberg, A.P., Poultney, C.S., Samocha, K., Cicek, A.E., Kou, Y., Liu, L., Fromer, M., Walker, S., et al.; DDD Study; Homozygosity Mapping Collaborative for Autism; UK10K Consortium (2014). Synaptic, transcriptional and chromatin genes disrupted in autism. Nature *515*, 209–215.

DePristo, M.A., Banks, E., Poplin, R., Garimella, K.V., Maguire, J.R., Hartl, C., Philippakis, A.A., del Angel, G., Rivas, M.A., Hanna, M., et al. (2011). A framework for variation discovery and genotyping using next-generation DNA sequencing data. Nat. Genet. *43*, 491–498.

Desmet, F.O., Hamroun, D., Lalande, M., Collod-Béroud, G., Claustres, M., and Béroud, C. (2009). Human Splicing Finder: an online bioinformatics tool to predict splicing signals. Nucleic Acids Res. *37*, e67.

Dong, C., Wei, P., Jian, X., Gibbs, R., Boerwinkle, E., Wang, K., and Liu, X. (2015). Comparison and integration of deleteriousness prediction methods for nonsynonymous SNVs in whole exome sequencing studies. Hum. Mol. Genet. *24*, 2125–2137.

Duncan, S.A., Manova, K., Chen, W.S., Hoodless, P., Weinstein, D.C., Bachvarova, R.F., and Darnell, J.E., Jr. (1994). Expression of transcription factor HNF-4 in the extraembryonic endoderm, gut, and nephrogenic tissue of the developing mouse embryo: HNF-4 is a marker for primary endoderm in the implanting blastocyst. Proc. Natl. Acad. Sci. USA *91*, 7598–7602.

Ecsedi, M., and Grosshans, H. (2013). LIN-41/TRIM71: emancipation of a miRNA target. Genes Dev. *27*, 581–589.

Eden, E., Navon, R., Steinfeld, I., Lipson, D., and Yakhini, Z. (2009). GOrilla: a tool for discovery and visualization of enriched GO terms in ranked gene lists. BMC Bioinformatics *10*, 48.

Eggenschwiler, J.T., and Anderson, K.V. (2007). Cilia and developmental signaling. Annu. Rev. Cell Dev. Biol. *23*, 345–373.

Eggenschwiler, J.T., Espinoza, E., and Anderson, K.V. (2001). Rab23 is an essential negative regulator of the mouse Sonic hedgehog signalling pathway. Nature *412*, 194–198.

Ekici, A.B., Hilfinger, D., Jatzwauk, M., Thiel, C.T., Wenzel, D., Lorenz, I., Boltshauser, E., Goecke, T.W., Staatz, G., Morris-Rosendahl, D.J., et al.

(2010). Disturbed Wnt Signalling due to a Mutation in CCDC88C Causes an Autosomal Recessive Non-Syndromic Hydrocephalus with Medial Diverticulum. Mol. Syndromol. *1*, 99–112.

Ellis, T., Smyth, I., Riley, E., Graham, S., Elliot, K., Narang, M., Kay, G.F., Wicking, C., and Wainwright, B. (2003). Patched 1 conditional null allele in mice. Genesis *36*, 158–161.

Ever, L., and Gaiano, N. (2005). Radial 'glial' progenitors: neurogenesis and signaling. Curr. Opin. Neurobiol. *15*, 29–33.

Feng, W., Choi, I., Clouthier, D.E., Niswander, L., and Williams, T. (2013). The Ptch1(DL) mouse: a new model to study lambdoid craniosynostosis and basal cell nevus syndrome-associated skeletal defects. Genesis *51*, 677–689.

Fischbach, G.D., and Lord, C. (2010). The Simons Simplex Collection: a resource for identification of autism genetic risk factors. Neuron *68*, 192–195.

Fromer, M., and Purcell, S.M. (2001). Using XHMM software to detect copy number variation in whole-exome sequencing data. Curr. Protoc. Hum. Genet. *81*, 7.23.1–7.23.21.

Fromer, M., Moran, J.L., Chambert, K., Banks, E., Bergen, S.E., Ruderfer, D.M., Handsaker, R.E., McCarroll, S.A., O'Donovan, M.C., Owen, M.J., et al. (2012). Discovery and statistical genotyping of copy-number variation from whole-exome sequencing depth. Am. J. Hum. Genet. *91*, 597–607.

Fromer, M., Pocklington, A.J., Kavanagh, D.H., Williams, H.J., Dwyer, S., Gormley, P., Georgieva, L., Rees, E., Palta, P., Ruderfer, D.M., et al. (2014). De novo mutations in schizophrenia implicate synaptic networks. Nature *506*, 179–184.

Fu, W., O'Connor, T.D., Jun, G., Kang, H.M., Abecasis, G., Leal, S.M., Gabriel, S., Rieder, M.J., Altshuler, D., Shendure, J., et al.; NHLBI Exome Sequencing Project (2013). Analysis of 6,515 exomes reveals the recent origin of most human protein-coding variants. Nature *493*, 216–220.

Garber, M., Guttman, M., Clamp, M., Zody, M.C., Friedman, N., and Xie, X. (2009). Identifying novel constrained elements by exploiting biased substitution patterns. Bioinformatics *25*, i54–i62.

Gavino, C., and Richard, S. (2011). Patched1 haploinsufficiency impairs ependymal cilia function of the quaking viable mice, leading to fatal hydrocephalus. Mol. Cell. Neurosci. *47*, 100–107.

Goodrich, L.V., Johnson, R.L., Milenkovic, L., McMahon, J.A., and Scott, M.P. (1996). Conservation of the hedgehog/patched signaling pathway from flies to mice: induction of a mouse patched gene by Hedgehog. Genes Dev. *10*, 301–312.

Goodrich, L.V., Milenković, L., Higgins, K.M., and Scott, M.P. (1997). Altered neural cell fates and medulloblastoma in mouse patched mutants. Science *277*, 1109–1113.

Gorlin, R.J. (2004). Nevoid basal cell carcinoma (Gorlin) syndrome. Genet. Med. *6*, 530–539.

Gorlin, R.J., and Goltz, R.W. (1960). Multiple nevoid basal-cell epithelioma, jaw cysts and bifid rib. A syndrome. N. Engl. J. Med. *262*, 908–912.

Govaert, P., Oostra, A., Matthys, D., Vanhaesebrouck, P., and Leroy, J. (1991). How idiopathic is idiopathic external hydrocephalus? Dev. Med. Child Neurol. *33*, 274–276.

Hahn, H., Wicking, C., Zaphiropoulous, P.G., Gailani, M.R., Shanley, S., Chidambaram, A., Vorechovsky, I., Holmberg, E., Unden, A.B., Gillies, S., et al. (1996). Mutations of the human homolog of Drosophila patched in the nevoid basal cell carcinoma syndrome. Cell *85*, 841–851.

Harmacek, L., Watkins-Chow, D.E., Chen, J., Jones, K.L., Pavan, W.J., Salbaum, J.M., and Niswander, L. (2014). A unique missense allele of BAF155, a core BAF chromatin remodeling complex protein, causes neural tube closure defects in mice. Dev. Neurobiol. *74*, 483–497.

Haverkamp, F., Wölfle, J., Aretz, M., Krämer, A., Höhmann, B., Fahnenstich, H., and Zerres, K. (1999). Congenital hydrocephalus internus and aqueduct stenosis: aetiology and implications for genetic counselling. Eur. J. Pediatr. *158*, 474–478.

Ho, L., Ronan, J.L., Wu, J., Staahl, B.T., Chen, L., Kuo, A., Lessard, J., Nesvizhskii, A.I., Ranish, J., and Crabtree, G.R. (2009). An embryonic stem cell chromatin remodeling complex, esBAF, is essential for embryonic stem cell self-renewal and pluripotency. Proc. Natl. Acad. Sci. USA *106*, 5181–5186.

Homsy, J., Zaidi, S., Shen, Y., Ware, J.S., Samocha, K.E., Karczewski, K.J., DePalma, S.R., McKean, D., Wakimoto, H., Gorham, J., et al. (2015). De novo mutations in congenital heart disease with neurodevelopmental and other congenital anomalies. Science *350*, 1262–1266.

Ioannidis, N.M., Rothstein, J.H., Pejaver, V., Middha, S., McDonnell, S.K., Baheti, S., Musolf, A., Li, Q., Holzinger, E., Karyadi, D., et al. (2016). REVEL: an ensemble method for predicting the pathogenicity of rare missense variants. Am. J. Hum. Genet. *99*, 877–885.

Ionita-Laza, I., McCallum, K., Xu, B., and Buxbaum, J.D. (2016). A spectral approach integrating functional genomic annotations for coding and noncoding variants. Nat. Genet. *48*, 214–220.

Iossifov, I., O'Roak, B.J., Sanders, S.J., Ronemus, M., Krumm, N., Levy, D., Stessman, H.A., Witherspoon, K.T., Vives, L., Patterson, K.E., et al. (2014). The contribution of de novo coding mutations to autism spectrum disorder. Nature *515*, 216–221.

Jagadeesh, K.A., Wenger, A.M., Berger, M.J., Guturu, H., Stenson, P.D., Cooper, D.N., Bernstein, J.A., and Bejerano, G. (2016). M-CAP eliminates a majority of variants of uncertain significance in clinical exomes at high sensitivity. Nat. Genet. *48*, 1581–1586.

Jessell, T.M., and Sanes, J.R. (2000). Development. The decade of the developing brain. Curr. Opin. Neurobiol. *10*, 599–611.

Jin, S.C., Homsy, J., Zaidi, S., Lu, Q., Morton, S., DePalma, S.R., Zeng, X., Qi, H., Chang, W., Sierant, M.C., et al. (2017). Contribution of rare inherited and de novo variants in 2,871 congenital heart disease probands. Nat. Genet. *49*, 1593–1601.

Kahle, K.T., Kulkarni, A.V., Limbrick, D.D., Jr., and Warf, B.C. (2016). Hydrocephalus in children. Lancet *387*, 788–799.

Kamuro, K., and Tenokuchi, Y. (1993). Familial periventricular nodular heterotopia. Brain Dev. *15*, 237–241.

Kanamoto, T., Terada, K., Yoshikawa, H., and Furukawa, T. (2006). Cloning and regulation of the vertebrate homologue of lin-41 that functions as a heterochronic gene in Caenorhabditis elegans. Dev. Dyn. *235*, 1142–1149.

Kent, W.J. (2002). BLAT–the BLAST-like alignment tool. Genome Res. *12*, 656–664.

Kim, J.K., Huh, S.O., Choi, H., Lee, K.S., Shin, D., Lee, C., Nam, J.S., Kim, H., Chung, H., Lee, H.W., et al. (2001). Srg3, a mouse homolog of yeast SWI3, is essential for early embryogenesis and involved in brain development. Mol. Cell. Biol. *21*, 7787–7795.

Kircher, M., Witten, D.M., Jain, P., O'Roak, B.J., Cooper, G.M., and Shendure, J. (2014). A general framework for estimating the relative pathogenicity of human genetic variants. Nat. Genet. *46*, 310–315.

Kousi, M., and Katsanis, N. (2016). The genetic basis of hydrocephalus. Annu. Rev. Neurosci. *39*, 409–435.

Krumm, N., Turner, T.N., Baker, C., Vives, L., Mohajeri, K., Witherspoon, K., Raja, A., Coe, B.P., Stessman, H.A., He, Z.-X., et al. (2015). Excess of rare, inherited truncating mutations in autism. Nat. Genet. *47*, 582–588.

Kumar, P., Henikoff, S., and Ng, P.C. (2009). Predicting the effects of coding non-synonymous variants on protein function using the SIFT algorithm. Nat. Protoc. *4*, 1073–1081.

Lek, M., Karczewski, K.J., Minikel, E.V., Samocha, K.E., Banks, E., Fennell, T., O'Donnell-Luria, A.H., Ware, J.S., Hill, A.J., Cummings, B.B., et al.; Exome Aggregation Consortium (2016). Analysis of protein-coding genetic variation in 60,706 humans. Nature *536*, 285–291.

Li, H., and Durbin, R. (2009). Fast and accurate short read alignment with Burrows-Wheeler transform. Bioinformatics *25*, 1754–1760.

Lindblad-Toh, K., Garber, M., Zuk, O., Lin, M.F., Parker, B.J., Washietl, S., Kheradpour, P., Ernst, J., Jordan, G., Mauceli, E., et al.; Broad Institute Sequencing Platform and Whole Genome Assembly Team; Baylor College of Medicine Human Genome Sequencing Center Sequencing Team; Genome Institute at Washington University (2011). A high-resolution map of human evolutionary constraint using 29 mammals. Nature *478*, 476–482.

Loedige, I., Gaidatzis, D., Sack, R., Meister, G., and Filipowicz, W. (2013). The mammalian TRIM-NHL protein TRIM71/LIN-41 is a repressor of mRNA function. Nucleic Acids Res. *41*, 518–532.

Loedige, I., Stotz, M., Qamar, S., Kramer, K., Hennig, J., Schubert, T., Löffler, P., Längst, G., Merkl, R., Urlaub, H., and Meister, G. (2014). The NHL domain of BRAT is an RNA-binding domain that directly contacts the hunchback mRNA for regulation. Genes Dev. *28*, 749–764.

Loedige, I., Jakob, L., Treiber, T., Ray, D., Stotz, M., Treiber, N., Hennig, J., Cook, K.B., Morris, Q., Hughes, T.R., et al. (2015). The crystal structure of the NHL domain in complex with RNA reveals the molecular basis of Drosophila brain-tumor-mediated gene regulation. Cell Rep. *13*, 1206–1220.

Lupo, G., Harris, W.A., and Lewis, K.E. (2006). Mechanisms of ventral patterning in the vertebrate nervous system. Nat. Rev. Neurosci. *7*, 103–114.

Maller Schulman, B.R., Liang, X., Stahlhut, C., DelConte, C., Stefani, G., and Slack, F.J. (2008). The let-7 microRNA target gene, Mlin41/Trim71 is required for mouse embryonic survival and neural tube closure. Cell Cycle *7*, 3935–3942.

Manichaikul, A., Mychaleckyj, J.C., Rich, S.S., Daly, K., Sale, M., and Chen, W.M. (2010). Robust relationship inference in genome-wide association studies. Bioinformatics *26*, 2867–2873.

Mazzola, C.A., Choudhri, A.F., Auguste, K.I., Limbrick, D.D., Jr., Rogido, M., Mitchell, L., and Flannery, A.M.; Pediatric Hydrocephalus Systematic Review and Evidence-Based Guidelines Task Force (2014). Pediatric hydrocephalus: systematic literature review and evidence-based guidelines. Part 2: management of posthemorrhagic hydrocephalus in premature infants. J. Neurosurg. Pediatr. *14* (*Suppl 1*), 8–23.

McAllister, J.P., 2nd, Williams, M.A., Walker, M.L., Kestle, J.R.W., Relkin, N.R., Anderson, A.M., Gross, P.H., and Browd, S.R.; Hydrocephalus Symposium Expert Panel (2015). An update on research priorities in hydrocephalus: overview of the third National Institutes of Health-sponsored symposium "Opportunities for Hydrocephalus Research: Pathways to Better Outcomes". J. Neurosurg. *123*, 1427–1438.

McAllister, J.P., Guerra, M.M., Ruiz, L.C., Jimenez, A.J., Dominguez-Pinos, D., Sival, D., den Dunnen, W., Morales, D.M., Schmidt, R.E., Rodriguez, E.M., and Limbrick, D.D. (2017). Ventricular zone disruption in human neonates with intraventricular hemorrhage. J. Neuropathol. Exp. Neurol. *76*, 358–375.

McKenna, A., Hanna, M., Banks, E., Sivachenko, A., Cibulskis, K., Kernytsky, A., Garimella, K., Altshuler, D., Gabriel, S., Daly, M., and DePristo, M.A. (2010). The Genome Analysis Toolkit: a MapReduce framework for analyzing next-generation DNA sequencing data. Genome Res. *20*, 1297–1303.

McPherson, E., and Clemens, M. (1997). Bruck syndrome (osteogenesis imperfecta with congenital joint contractures): review and report on the first North American case. Am. J. Med. Genet. *70*, 28–31.

Merkle, F.T., Tramontin, A.D., García-Verdugo, J.M., and Alvarez-Buylla, A. (2004). Radial glia give rise to adult neural stem cells in the subventricular zone. Proc. Natl. Acad. Sci. USA *101*, 17528–17532.

Milenkovic, L., Goodrich, L.V., Higgins, K.M., and Scott, M.P. (1999). Mouse patched1 controls body size determination and limb patterning. Development *126*, 4431–4440.

Mitschka, S., Ulas, T., Goller, T., Schneider, K., Egert, A., Mertens, J., Brüstle, O., Schorle, H., Beyer, M., Klee, K., et al. (2015). Co-existence of intact stemness and priming of neural differentiation programs in mES cells lacking Trim71. Sci. Rep. *5*, 11126.

Munch, T.N., Rostgaard, K., Rasmussen, M.L., Wohlfahrt, J., Juhler, M., and Melbye, M. (2012). Familial aggregation of congenital hydrocephalus in a nationwide cohort. Brain *135*, 2409–2415.

Narayanan, R., Pirouz, M., Kerimoglu, C., Pham, L., Wagener, R.J., Kiszka, K.A., Rosenbusch, J., Seong, R.H., Kessel, M., Fischer, A., et al. (2015). Loss of BAF (mSWI/SNF) complexes causes global transcriptional and chromatin state changes in forebrain development. Cell Rep. *13*, 1842–1854.

Neale, B.M., Kou, Y., Liu, L., Ma'ayan, A., Samocha, K.E., Sabo, A., Lin, C.F., Stevens, C., Wang, L.S., Makarov, V., et al. (2012). Patterns and rates of exonic de novo mutations in autism spectrum disorders. Nature *485*, 242–245.

Ng, P.C., and Henikoff, S. (2001). Predicting deleterious amino acid substitutions. Genome Res. *11*, 863–874.

Ng, P.C., and Henikoff, S. (2002). Accounting for human polymorphisms predicted to affect protein function. Genome Res. *12*, 436–446.

Ng, P.C., and Henikoff, S. (2003). SIFT: Predicting amino acid changes that affect protein function. Nucleic Acids Res. *31*, 3812–3814.

Ng, P.C., and Henikoff, S. (2006). Predicting the effects of amino acid substitutions on protein function. Annu. Rev. Genomics Hum. Genet. *7*, 61–80.

Nguyen, H., Sokpor, G., Pham, L., Rosenbusch, J., Stoykova, A., Staiger, J.F., and Tuoc, T. (2016). Epigenetic regulation by BAF (mSWI/SNF) chromatin remodeling complexes is indispensable for embryonic development. Cell Cycle *15*, 1317–1324.

Nguyen, D.T.T., Richter, D., Michel, G., Mitschka, S., Kolanus, W., Cuevas, E., and Wulczyn, F.G. (2017). The ubiquitin ligase LIN41/TRIM71 targets p53 to antagonize cell death and differentiation pathways during stem cell differentiation. Cell Death Differ. *24*, 1063–1078.

Noctor, S.C., Martínez-Cerdeño, V., Ivic, L., and Kriegstein, A.R. (2004). Cortical neurons arise in symmetric and asymmetric division zones and migrate through specific phases. Nat. Neurosci. *7*, 136–144.

O'Roak, B.J., Deriziotis, P., Lee, C., Vives, L., Schwartz, J.J., Girirajan, S., Karakoc, E., Mackenzie, A.P., Ng, S.B., Baker, C., et al. (2011). Exome sequencing in sporadic autism spectrum disorders identifies severe de novo mutations. Nat. Genet. *43*, 585–589.

Palma, V., and Ruiz i Altaba, A. (2004). Hedgehog-GLI signaling regulates the behavior of cells with stem cell properties in the developing neocortex. Development *131*, 337–345.

Palma, V., Lim, D.A., Dahmane, N., Sánchez, P., Brionne, T.C., Herzberg, C.D., Gitton, Y., Carleton, A., Álvarez-Buylla, A., and Ruiz i Altaba, A. (2005). Sonic hedgehog controls stem cell behavior in the postnatal and adult brain. Development *132*, 335–344.

Petersen, P.H., Zou, K., Hwang, J.K., Jan, Y.N., and Zhong, W. (2002). Progenitor cell maintenance requires numb and numblike during mouse neurogenesis. Nature *419*, 929–934.

Pollard, K.S., Hubisz, M.J., Rosenbloom, K.R., and Siepel, A. (2010). Detection of nonneutral substitution rates on mammalian phylogenies. Genome Res. *20*, 110–121.

Price, A.L., Patterson, N.J., Plenge, R.M., Weinblatt, M.E., Shadick, N.A., and Reich, D. (2006). Principal components analysis corrects for stratification in genome-wide association studies. Nat. Genet. *38*, 904–909.

Purcell, S., Neale, B., Todd-Brown, K., Thomas, L., Ferreira, M.A., Bender, D., Maller, J., Sklar, P., de Bakker, P.I., Daly, M.J., and Sham, P.C. (2007). PLINK: a tool set for whole-genome association and population-based linkage analyses. Am. J. Hum. Genet. *81*, 559–575.

Quang, D., Chen, Y., and Xie, X. (2015). DANN: a deep learning approach for annotating the pathogenicity of genetic variants. Bioinformatics *31*, 761–763.

Reinhart, B.J., Slack, F.J., Basson, M., Pasquinelli, A.E., Bettinger, J.C., Rougvie, A.E., Horvitz, H.R., and Ruvkun, G. (2000). The 21-nucleotide let-7 RNA regulates developmental timing in Caenorhabditis elegans. Nature *403*, 901–906.

Rekate, H.L. (2008). The definition and classification of hydrocephalus: a personal recommendation to stimulate debate. Cerebrospinal Fluid Res. *5*, 2.

Reva, B., Antipin, Y., and Sander, C. (2011). Predicting the functional impact of protein mutations: application to cancer genomics. Nucleic Acids Res. *39*, e118.

Robinson, S. (2012). Neonatal posthemorrhagic hydrocephalus from prematurity: pathophysiology and current treatment concepts. J. Neurosurg. Pediatr. *9*, 242–258.

Robinson, J.T., Thorvaldsdóttir, H., Winckler, W., Guttman, M., Lander, E.S., Getz, G., and Mesirov, J.P. (2011). Integrative genomics viewer. Nat. Biotechnol. *29*, 24–26.

Rosenthal, A., Jouet, M., and Kenwrick, S. (1992). Aberrant splicing of neural cell adhesion molecule L1 mRNA in a family with X-linked hydrocephalus. Nat. Genet. *2*, 107–112.

Ruderfer, D.M., Hamamsy, T., Lek, M., Karczewski, K.J., Kavanagh, D., Samocha, K.E., Daly, M.J., MacArthur, D.G., Fromer, M., and Purcell, S.M.; Exome Aggregation Consortium (2016). Patterns of genic intolerance of rare copy number variation in 59,898 human exomes. Nat. Genet. *48*, 1107–1111.

Samocha, K.E., Robinson, E.B., Sanders, S.J., Stevens, C., Sabo, A., McGrath, L.M., Kosmicki, J.A., Rehnström, K., Mallick, S., Kirby, A., et al. (2014). A framework for the interpretation of de novo mutation in human disease. Nat. Genet. *46*, 944–950.

Samocha, K.E., Kosmicki, J.A., Karczewski, K.J., O'Donnell-Luria, A.H., Pierce-Hoffman, E., MacArthur, D.G., Neale, B.M., and Daly, M.J. (2017). Regional missense constraint improves variant deleteriousness prediction. bioRxiv https://doi.org/10.1101/148353.

Sanders, S.J., Murtha, M.T., Gupta, A.R., Murdoch, J.D., Raubeson, M.J., Willsey, A.J., Ercan-Sencicek, A.G., DiLullo, N.M., Parikshak, N.N., Stein, J.L., et al. (2012). De novo mutations revealed by whole-exome sequencing are strongly associated with autism. Nature *485*, 237–241.

Schaeren-Wiemers, N., and Gerfin-Moser, A. (1993). A single protocol to detect transcripts of various types and expression levels in neural tissue and cultured cells: in situ hybridization using digoxigenin-labelled cRNA probes. Histochemistry *100*, 431–440.

Schulman, B.R., Esquela-Kerscher, A., and Slack, F.J. (2005). Reciprocal expression of lin-41 and the microRNAs let-7 and mir-125 during mouse embryogenesis. Dev. Dyn. *234*, 1046–1054.

Schwarz, J.M., Rödelsperger, C., Schuelke, M., and Seelow, D. (2010). MutationTaster evaluates disease-causing potential of sequence alterations. Nat. Methods *7*, 575–576.

Shaheen, R., Sebai, M.A., Patel, N., Ewida, N., Kurdi, W., Altweijri, I., Sogaty, S., Almardawi, E., Seidahmed, M.Z., Alnemri, A., et al. (2017). The genetic landscape of familial congenital hydrocephalus. Ann. Neurol. *81*, 890–897.

Shannon, C.N., Simon, T.D., Reed, G.T., Franklin, F.A., Kirby, R.S., Kilgore, M.L., and Wellons, J.C., 3rd (2011). The economic impact of ventriculoperitoneal shunt failure. J. Neurosurg. Pediatr. *8*, 593–599.

Sheen, V.L., Basel-Vanagaite, L., Goodman, J.R., Scheffer, I.E., Bodell, A., Ganesh, V.S., Ravenscroft, R., Hill, R.S., Cherry, T.J., Shugart, Y.Y., et al. (2004). Etiological heterogeneity of familial periventricular heterotopia and hydrocephalus. Brain Dev. *26*, 326–334.

Sherry, S.T., Ward, M.H., Kholodov, M., Baker, J., Phan, L., Smigielski, E.M., and Sirotkin, K. (2001). dbSNP: the NCBI database of genetic variation. Nucleic Acids Res. *29*, 308–311.

Shihab, H.A., Gough, J., Cooper, D.N., Stenson, P.D., Barker, G.L., Edwards, K.J., Day, I.N., and Gaunt, T.R. (2013). Predicting the functional, molecular, and phenotypic consequences of amino acid substitutions using hidden Markov models. Hum. Mutat. *34*, 57–65.

Shihab, H.A., Gough, J., Mort, M., Cooper, D.N., Day, I.N., and Gaunt, T.R. (2014). Ranking non-synonymous single nucleotide polymorphisms based on disease concepts. Hum. Genomics *8*, 11.

Shihab, H.A., Rogers, M.F., Gough, J., Mort, M., Cooper, D.N., Day, I.N.M., Gaunt, T.R., and Campbell, C. (2015). An integrative approach to predicting the functional effects of non-coding and coding sequence variation. Bioinformatics *31*, 1536–1543.

Shikata, Y., Okada, T., Hashimoto, M., Ellis, T., Matsumaru, D., Shiroishi, T., Ogawa, M., Wainwright, B., and Motoyama, J. (2011). Ptch1-mediated dosage-dependent action of Shh signaling regulates neural progenitor development at late gestational stages. Dev. Biol. *349*, 147–159.

Siepel, A., Bejerano, G., Pedersen, J.S., Hinrichs, A.S., Hou, M., Rosenbloom, K., Clawson, H., Spieth, J., Hillier, L.W., Richards, S., et al. (2005). Evolutionarily conserved elements in vertebrate, insect, worm, and yeast genomes. Genome Res. *15*, 1034–1050.

Simon, T.D., Riva-Cambrin, J., Srivastava, R., Bratton, S.L., Dean, J.M., and Kestle, J.R.; Hydrocephalus Clinical Research Network (2008). Hospital care for children with hydrocephalus in the United States: utilization, charges, comorbidities, and deaths. J. Neurosurg. Pediatr. *1*, 131–137.

Slack, F.J., and Ruvkun, G. (1998). A novel repeat domain that is often associated with RING finger and B-box motifs. Trends Biochem. Sci. *23*, 474–475.

Slack, F.J., Basson, M., Liu, Z., Ambros, V., Horvitz, H.R., and Ruvkun, G. (2000). The lin-41 RBCC gene acts in the C. elegans heterochronic pathway between the let-7 regulatory RNA and the LIN-29 transcription factor. Mol. Cell *5*, 659–669.

Slavotinek, A., Kaylor, J., Pierce, H., Cahr, M., DeWard, S.J., Schneidman-Duhovny, D., Alsadah, A., Salem, F., Schmajuk, G., and Mehta, L. (2015). CRB2 mutations produce a phenotype resembling congenital nephrosis, Finnish type, with cerebral ventriculomegaly and raised alpha-fetoprotein. Am. J. Hum. Genet. *96*, 162–169.

Stuart, B.D., Choi, J., Zaidi, S., Xing, C., Holohan, B., Chen, R., Choi, M., Dharwadkar, P., Torres, F., Girod, C.E., et al. (2015). Exome sequencing links mutations in PARN and RTEL1 with familial pulmonary fibrosis and telomere shortening. Nat. Genet. *47*, 512–517.

Deciphering Developmental Disorders Study (2015). Large-scale discovery of novel genetic causes of developmental disorders. Nature *519*, 223–228.

Deciphering Developmental Disorders Study (2017). Prevalence and architecture of de novo mutations in developmental disorders. Nature *542*, 433–438.

Sudmant, P.H., Rausch, T., Gardner, E.J., Handsaker, R.E., Abyzov, A., Huddleston, J., Zhang, Y., Ye, K., Jun, G., Fritz, M.H.-Y., et al.; 1000 Genomes Project Consortium (2015). An integrated map of structural variation in 2,504 human genomes. Nature *526*, 75–81.

Svärd, J., Rozell, B., Toftgård, R., and Teglund, S. (2009). Tumor suppressor gene co-operativity in compound Patched1 and suppressor of fused heterozygous mutant mice. Mol. Carcinog. *48*, 408–419.

Takahashi, M., and Osumi, N. (2002). Pax6 regulates specification of ventral neurone subtypes in the hindbrain by establishing progenitor domains. Development *129*, 1327–1338.

Timberlake, A.T., Choi, J., Zaidi, S., Lu, Q., Nelson-Williams, C., Brooks, E.D., Bilguvar, K., Tikhonova, I., Mane, S., Yang, J.F., et al. (2016). Two locus inheritance of non-syndromic midline craniosynostosis via rare *SMAD6* and common *BMP2* alleles. eLife *5*, 5.

Timberlake, A.T., Furey, C.G., Choi, J., Nelson-Williams, C., Loring, E., Galm, A., Kahle, K.T., Steinbacher, D.M., Larysz, D., Persing, J.A., and Lifton, R.P.; Yale Center for Genome Analysis (2017). De novo mutations in inhibitors of Wnt, BMP, and Ras/ERK signaling pathways in non-syndromic midline craniosynostosis. Proc. Natl. Acad. Sci. USA *114*, E7341–E7347.

Tissir, F., Qu, Y., Montcouquiol, M., Zhou, L., Komatsu, K., Shi, D., Fujimori, T., Labeau, J., Tyteca, D., Courtoy, P., et al. (2010). Lack of cadherins Celsr2 and Celsr3 impairs ependymal ciliogenesis, leading to fatal hydrocephalus. Nat. Neurosci. *13*, 700–707.

Tully, H.M., and Dobyns, W.B. (2014). Infantile hydrocephalus: a review of epidemiology, classification and causes. Eur. J. Med. Genet. *57*, 359–368.

Tully, H.M., Ishak, G.E., Rue, T.C., Dempsey, J.C., Browd, S.R., Millen, K.J., Doherty, D., and Dobyns, W.B. (2016). Two hundred thirty-six children with developmental hydrocephalus: causes and clinical consequences. J. Child Neurol. *31*, 309–320.

Tuoc, T.C., Boretius, S., Sansom, S.N., Pitulescu, M.E., Frahm, J., Livesey, F.J., and Stoykova, A. (2013a). Chromatin regulation by BAF170 controls cerebral cortical size and thickness. Dev. Cell *25*, 256–269.

Tuoc, T.C., Narayanan, R., and Stoykova, A. (2013b). BAF chromatin remodeling complex: cortical size regulation and beyond. Cell Cycle *12*, 2953–2959.

Van der Auwera, G.A., Carneiro, M.O., Hartl, C., Poplin, R., Del Angel, G., Levy-Moonshine, A., Jordan, T., Shakir, K., Roazen, D., Thibault, J., et al. (2013). From FastQ data to high confidence variant calls: the Genome Analysis Toolkit best practices pipeline. Curr. Protoc. Bioinformatics *43*, 1–33, 33.

Vella, M.C., Choi, E.Y., Lin, S.Y., Reinert, K., and Slack, F.J. (2004). The C. elegans microRNA let-7 binds to imperfect let-7 complementary sites from the lin-41 3'UTR. Genes Dev. *18*, 132–137.

Wang, W., Xue, Y., Zhou, S., Kuo, A., Cairns, B.R., and Crabtree, G.R. (1996). Diversity and specialization of mammalian SWI/SNF complexes. Genes Dev. *10*, 2117–2130.

Wang, C., Pan, Y., and Wang, B. (2010a). Suppressor of fused and Spop regulate the stability, processing and function of Gli2 and Gli3 full-length activators but not their repressors. Development *137*, 2001–2009.

Wang, K., Li, M., and Hakonarson, H. (2010b). ANNOVAR: functional annotation of genetic variants from high-throughput sequencing data. Nucleic Acids Res. *38*, e164.

Ware, J.S., Samocha, K.E., Homsy, J., and Daly, M.J. (2015). Interpreting de novo variation in human disease using denovolyzeR. Curr. Protoc. Hum. Genet. *87*, 1–15, 15.

Wetmore, C., Eberhart, D.E., and Curran, T. (2000). The normal patched allele is expressed in medulloblastomas from mice with heterozygous germ-line mutation of patched. Cancer Res. *60*, 2239–2246.

Wetmore, K.M., Price, M.N., Waters, R.J., Lamson, J.S., He, J., Hoover, C.A., Blow, M.J., Bristow, J., Butland, G., Arkin, A.P., and Deutschbauer, A. (2015). Rapid quantification of mutant fitness in diverse bacteria by sequencing randomly bar-coded transposons. MBio *6*, e00306–e00315.

Worringer, K.A., Rand, T.A., Hayashi, Y., Sami, S., Takahashi, K., Tanabe, K., Narita, M., Srivastava, D., and Yamanaka, S. (2014). The let-7/LIN-41 pathway regulates reprogramming to human induced pluripotent stem cells by controlling expression of prodifferentiation genes. Cell Stem Cell *14*, 40–52.

Yan, Z., Wang, Z., Sharova, L., Sharov, A.A., Ling, C., Piao, Y., Aiba, K., Matoba, R., Wang, W., and Ko, M.S. (2008). BAF250B-associated SWI/SNF chromatin-remodeling complex is required to maintain undifferentiated mouse embryonic stem cells. Stem Cells *26*, 1155–1165.

Yao, B., Christian, K.M., He, C., Jin, P., Ming, G.L., and Song, H. (2016). Epigenetic mechanisms in neurogenesis. Nat. Rev. Neurosci. *17*, 537–549.

Yeo, G., and Burge, C.B. (2004). Maximum entropy modeling of short sequence motifs with applications to RNA splicing signals. J. Comp. Biol *11*, 377–394.

Yu, G., Yang, Y., and Tian, G. (2010). Expressing and characterization of mLIN-41 in mouse early embryos and adult muscle tissues. J. Mol. Histol. *41*, 295–305.

Yung, Y.C., Mutoh, T., Lin, M.-E., Noguchi, K., Rivera, R.R., Choi, J.W., Kingsbury, M.A., and Chun, J. (2011). Lysophosphatidic acid signaling may initiate fetal hydrocephalus. Sci. Transl. Med. *3*, 99ra87.

Zaidi, S., Choi, M., Wakimoto, H., Ma, L., Jiang, J., Overton, J.D., Romano-Adesman, A., Bjornson, R.D., Breitbart, R.E., Brown, K.K., et al. (2013). De novo mutations in histone-modifying genes in congenital heart disease. Nature *498*, 220–223.

Zega, K., Jovanovic, V.M., Vitic, Z., Niedzielska, M., Knaapi, L., Jukic, M.M., Partanen, J., Friedel, R.H., Lang, R., and Brodski, C. (2017). Dusp16 deficiency causes congenital obstructive hydrocephalus and brain overgrowth by expansion of the neural progenitor pool. Front. Mol. Neurosci. *10*, 372.

Zhang, J., Williams, M.A., and Rigamonti, D. (2006). Genetics of human hydrocephalus. J. Neurol. *253*, 1255–1266.

STAR★METHODS

KEY RESOURCES TABLE

REAGENT or RESOURCE	SOURCE	IDENTIFIER
Deposited Data		
Whole-exome sequencing data from CH trios (n = 125)	This paper	dbGaP: phs000744; https://www.ncbi.nlm.nih.gov/projects/gap/cgi-bin/study.cgi?study_id=phs000744
Whole-exome sequencing data from SSC control trios	Iossifov et al., 2014	https://ndar.nih.gov/study.html?id=352
Software and Algorithms		
Genome Analysis Tool Kit (GATK)	DePristo et al., 2011; McKenna et al., 2010; Van der Auwera et al., 2013	https://software.broadinstitute.org/gatk/
BWA-mem	Li and Durbin, 2009	http://bio-bwa.sourceforge.net/
Annovar	Wang et al., 2010b	http://annovar.openbioinformatics.org/en/latest/
PLINK/SEQ	Fromer et al., 2014	https://atgu.mgh.harvard.edu/plinkseq/
Other		
1000 Genomes GRCh37 h19 genome build	1000 Genomes Project	http://ftp.1000genomes.ebi.ac.uk/vol1/ftp/technical/reference/human_g1k_v37.fasta.gz
RefSeq hg19 gene annotation	UCSC Genome Browser	http://genome.ucsc.edu/cgi-bin/hgTables?command=start
Intervals file for IDT xGen v.1.0	Integrated DNA Technologies	http://www.idtdna.com/pages/products/next-generation-sequencing/hybridization-capture/lockdown-panels/xgen-exome-research-panel

CONTACT FOR REAGENT AND RESOURCE SHARING

Further information and requests for resources and reagents should be directed to and will be fulfilled by the Lead Contact, Dr. Kristopher T. Kahle (kristopher.kahle@yale.edu).

EXPERIMENTAL MODEL AND SUBJECT DETAILS

Subjects and Samples

All study procedures and protocols comply with Yale University's Human Investigation Committee and Human Research Protection Program. Written informed consent for genetic studies was obtained from all participants. Inclusion criteria included patients with primary congenital hydrocephalus without known genetic causes such as *L1CAM* or any other large chromosomal deletions or re-arrangements. Hydrocephalus cases with secondarily acquired etiologies such as intraventricular hemorrhage (IVH), meningitis, obstruction due to tumors or cysts, and stroke were excluded. Children with hydranencephaly, large cysts and cephaloceles, posterior fossa crowding, myelomeningocele (Chiari II syndrome), or benign extra-axial CSF accumulation (i.e., benign external hydrocephalus) were also excluded. Sequenced trios were composed of two unaffected parents and one affected child with primary congenital hydrocephalus. All probands had undergone surgery for therapeutic CSF diversion (shunt placement and/or endoscopic third ventriculostomy). Patients and participating family members provided buccal swab samples (Isohelix SK-2S DNA buccal swab kits), medical records, radiological imaging studies, operative reports, and congenital hydrocephalus phenotype data.

The control cohort was composed of 1,789 previously whole-exome sequenced and analyzed families from the Simons Foundation Autism Research Initiative Simplex Collection (Fischbach and Lord, 2010; Iossifov et al., 2014; Krumm et al., 2015; O'Roak et al., 2011; Sanders et al., 2012). Sequenced families were comprised of two unaffected parents, one affected child with autism, and one unaffected sibling. Only the unaffected sibling and parents, as designated by the Simons Simplex Collection, were analyzed and served as controls for this study (Krumm et al., 2015).

Whole-Exome Sequencing and Variant Calling

DNA was isolated from buccal swab samples in accordance with manufacturer protocol. Whole-exome sequencing was performed using the IDT xGen capture reagent followed by 99 base paired-end sequencing on the Illumina HiSeq 2000 instrument at the Yale Center for Genome Analysis as previously described (Timberlake et al., 2016). Exome sequencing quality metrics are shown in Table S2 and Figures S1 and S2.

Sequence reads were mapped and aligned to the GRCh37/hg19 human reference genome using Burrows-Wheeler Aligner-MEM (Li and Durbin, 2009). In accordance with GATK Best Practices recommendations, the data were further processed using Genome Analysis Toolkit (GATK) base quality score recalibration (McKenna et al., 2010), indel realignment, duplication marking and removal, and base quality score recalibration (DePristo et al., 2011; Van der Auwera et al., 2013). Single nucleotide variants and small insertions and deletion were called using GATK Haplotype Caller and annotated using ANNOVAR (Wang et al., 2010b), NHLBI exome variant server (Fu et al., 2013), 1000 Genomes (Auton et al., 2015), DbSNP (Sherry et al., 2001), and gnomAD and ExAC databases (Lek et al., 2016).

The average depth of coverage of the whole-exome sequencing data was 54.3x, with greater than 8x coverage in 95.9% of the target region for exome capture (Table S2).

The sporadic or autosomal recessive mode of inheritance exhibited in our cohort pedigrees led us to prioritize *de novo*, compound heterozygous, and homozygous variants. Variants were filtered for predicted deleteriousness and conservation using a series of *in silico* prediction algorithms, including Meta-analytic support vector machine (MetaSVM) and Meta-analytic logistic regression (MetaLR) (Dong et al., 2015), Polymorphism Phenotyping (PolyPhen) (Adzhubei et al., 2010), Combined Annotation-Dependent Depletion (CADD) (Kircher et al., 2014), Sorting Intolerant From Tolerant (SIFT) (Kumar et al., 2009; Ng and Henikoff, 2001, 2002, 2003, 2006), conservation across 46 orthologs (cons46diff) (Cromer et al., 2012; Stuart et al., 2015), Likelihood Ratio Test (LRT) (Chun and Fay, 2009), MutationTaster (Schwarz et al., 2010), Mutation Assessor (Reva et al., 2011), Functional Analysis Through Hidden Markov Models (FATHMM) (Shihab et al., 2013), FATHMM–Multiple Kernel Learning (FATHMM-MKL) (Shihab et al., 2015), FATHMM-Coding (Shihab et al., 2014), Protein Variant Effect Analyzer (PROVEAN) (Choi et al., 2012), Variant Effect Scoring Tool (VEST3) (Carter et al., 2013), Mendelian Clinically Applicable Pathogenicity (M-CAP) (Jagadeesh et al., 2016), deleterious annotation of genetic variants using neural networks (DANN) (Quang et al., 2015), Eigen-PC (Ionita-Laza et al., 2016), Genomic Evolutionary Rate Profiling (GERP++ and GERPP++ GT2) (Davydov et al., 2010), phylogenetic p values (phyloP100way and phyloP20way) (Pollard et al., 2010), phastCons100way and phastCons20way (Siepel et al., 2005), Site-specific Phylogenetic analysis (SiPhy) (Garber et al., 2009; Lindblad-Toh et al., 2011), REVEL (Ioannidis et al., 2016), and MPC (Samocha et al., 2017).

METHOD DETAILS

Kinship Analysis

Pedigree information and participant relationships were confirmed utilizing pairwise PLINK identity-by-descent (IBD) calculation (Purcell et al., 2007). The IBD sharing between the probands and parents in all trios is between 45% and 55%. Pairwise individual relatedness was corroborated using KING (Manichaikul et al., 2010).

Haplotype Phasing and Analysis of Inbreeding

Haplotype phasing, inbreeding coefficient, and the longest homozygosity-by-descent (HBD) fragment were estimated using Beagle v3.3.2 (Browning and Browning, 2007) as described previously (Jin et al., 2017). The criteria of consanguinity are defined as runs of homozygosity in segments of 2cM or greater length that collectively comprise at least 0.35% of the genome.

Principal Component Analysis

In order to determine the ethnicity of each participant, we utilized the EIGENSTRAT software (Price et al., 2006) to analyze SNPs in cases, controls, and HapMap subjects as previously described (Jin et al., 2017; Timberlake et al., 2016).

De Novo and Inherited Variant Analysis and Filtering

De novo mutations were called in parent-offspring trios, each consisting of an affected child with primary congenital hydrocephalus and his or her unaffected biological parents, using the Bayesian framework TrioDeNovo (Dong et al., 2015). Candidate *de novo* variants were filtered based on the following criteria: (1) minor allele frequency (MAF) $\leq 5 \times 10^{-3}$ in ExAC, 1000 Genomes, and EVS, (2) GATK variant quality score recalibration (VQSR) of 'pass', (3) minimum sequencing depth of 8 reads in the proband and each parent, (4) genotype quality (GQ) score ≥ 20 and alternate allele ratio $\geq 40\%$, (5) TrioDeNovo data quality (DQ) score ≥ 7, and (6) exonic or splice-site variant.

Transmitted dominant variants were filtered by similar criteria of rareness and quality: (1) MAF $\leq 2 \times 10^{-5}$ in ExAC, (2) GQ ≥ 20 and alternate allele ratio $\geq 40\%$, (3) GATK VQSR of 'pass', and (4) minimum sequencing depth of 8 reads in each participant. Recessive variants were also filtered for rare (MAF $\leq 10^{-3}$ in ExAC) bi-allelic events (homozygous and compound heterozygous mutations) that met read quality criteria as above (GQ ≥ 20, alternate allele ratio $\geq 40\%$, 'pass' GATK VQSR, and minimum sequencing depth ≥ 8). Hemizygous recessive variants were filtered for rare events (MAF $\leq 2 \times 10^{-5}$) using the same quality criteria described above.

The impact of nonsynonymous single nucleotide variants on protein function was predicted using the MetaSVM algorithm (Dong et al., 2015), identifying mutations with rank scores greater than 0.83357 as deleterious ('D-mis'). D-Mis and loss-of function mutations (nonsense, frameshift insertions and deletions, and splice-site) were considered potentially damaging to protein function.

All *de novo* and transmitted calls were verified by *in silico* visualization of aligned reads using the BLAT search (Kent, 2002) and Integrative Genomics Viewer (IGV) (Robinson et al., 2011). Salient *de novo* and compound heterozygous calls were then verified in all participants that provided DNA by direct Sanger sequencing of PCR amplicons containing the mutation.

Burden of *De Novo* Mutations

The burden of *de novo* mutations in congenital hydrocephalus cases and unaffected autism controls was determined using the denovolyzeR package (Ware et al., 2015) as previously described The probability of observing a *de novo* mutation in each gene was calculated as illustrated previously (Jin et al., 2017), with the exception that the coverage adjustment factor was based on the full set of 125 case trios (or 126 case trios in the *SMARCC1* analysis given the inclusion of a *de novo* in parent Hydro106-3) and 1,789 control trios (separate probability tables for each set). The expected number of *de novo* mutations across variant classes in case and control cohorts was calculated and compared to the observed number of *de novo* mutations in each cohort using the Poisson test (Samocha et al., 2014). Gene-set enrichment analyses and statistical tests considered only mutations observed or expected in genes within the specified set (i.e., high brain-expressed, aqueductal stenosis).

Contribution of *De Novo* Mutation to Congenital Hydrocephalus

The number of *de novo* mutations in risk genes that contribute to congenital hydrocephalus was calculated based on the observed count of protein-altering *de novo* mutations compared to expectation (= $Nx((M_1–M_2)/M_1)$, where N is the total number of trios and M_1 and M_2 are the observed and expected count of protein-altering *de novo* mutations per trio, respectively)

Enrichment Analysis for the Dominant and Recessive Variants

To quantify the enrichment of LOF heterozygous variants, we calculated the expectation for a gene using the following formula:

$$\text{Expected LOF}_j = L \times \frac{\text{mutability}_j}{\sum_{Genes}\text{mutability}_j}$$

where 'j' denotes the 'jth' gene and 'L' denotes the total number of LOF heterozygous mutations. A one-tailed binomial test was conducted to compare the observed number of heterozygous variants to expectation.

For damaging recessive genotypes (RGs) in a specific gene in cases, we conducted a one-tailed binomial test to evaluate enrichment as described previously (Jin et al., 2017). RG can also be modeled separately as compound heterozygotes or homozygotes. The expected number of compound heterozygotes for each gene is derived from distributing the observed number of RGs, N, across all genes according to the ratio of the squared *de novo* probabilities:

$$\text{Expected Compound RG}_i = N \times \frac{probability^2_{de\ novo}}{\sum_{Genes}\left(probability^2_{de\ novo}\right)}$$

The expected number of homozygotes is derived similarly, but using the linear ratio of *de novo* probabilities:

$$\text{Expected Homozygous RG}_i = N \times \frac{probability_{de\ novo}}{\sum_{Genes}\left(probability_{de\ novo}\right)}$$

The total number of expected RG for each gene is the sum of the derived expected compound heterozygous and homozygous values.

Gene Ontology Enrichment Analysis

Three genome-wide significant genes *PTCH1*, *SMARCC1*, and *TRIM71* were input into GOrilla (Eden et al., 2009) to identify enriched GO terms compared to the background set of genes (M = 18,715). For gene-set enrichment analyses, each statistical test considered observed or expected mutations in genes within the specified gene set.

In Silico Splice-Site Prediction

In order to assess the impact of a missense mutation at the splice donor site of intron 10 of *PTCH1* that changed the donor site sequenced from GTA to GTC, we utilized Human Splicing Finder (Desmet et al., 2009) and MaxEntScan (Yeo and Burge, 2004). Both programs predicted that this mutation is likely to affect splicing. MaxEntScan assigned a MaxEnt score of 7.64 to the wild-type canonical splice donor site; however, after mutation of the wild-type sequence to GTC, the alternate splice donor bases upstream was assigned a score of −0.18. The difference in MaxEnt scores between the mutant and the reference sequence is −7.82, which provides strong support for this mutation being a potential 5′ donor splice site.

Copy Number Variation Analysis

XHMM was run to call CNVs from WES as previously described (Ruderfer et al., 2016). GATK DepthOfCoverage was used to calculate mean read depth per targets from the alignment files. The data were normalized by removing the highest variance principal components (variance > 70%) and z scores were calculated from the mean read depths. CNVs were called using the Viterbi Hidden Markov model (HMM) and the quality scores were calculated using the forward-backward HMM. After filtering out common CNVs present at allele frequencies greater than 0.1% in 1000 Genomes (Sudmant et al., 2015) and 10% in the cohort, high quality CNVs (SQ > 60 where SQ indicates the phred-scaled quality score for the presence of a CNV event within the interval) were subjected to visual inspection. *De novo* CNVs were assessed using PLINK/Seq command-line tools (Fromer et al., 2012).

QUANTIFICATION AND STATISTICAL ANALYSIS

De Novo CNV Permutation Test

The probability of finding one exon covered by multiple *de novo* CNVs was calculated by comparing the observed distribution to an empirical distribution derived from 1 million permutations. For each permutation, five *de novo* duplications were randomly distributed across the genome; each duplication contained the same number of exons as predicted from XHMM with adjustment if the CNV is partially validated by experiment. In each permutation, the experiment was considered a success if at least one locus contained exactly one exon was covered by multiple duplications. The number of successes was tallied and the p value was obtained by dividing the number of successes by the number of iterations.

Estimating the Number of Risk Genes

A maximum likelihood approach was used to estimate the number of genes contributing to congenital hydrocephalus via *de novo* events as described previously (Jin et al., 2017). We defined K to be the number of observed protein-altering *de novo* mutations in high brain-expressed (HBE) genes among cases. R1 indicates the number of HBE genes mutated exactly twice in cases and R2 indicates the number of high HBE mutated three times or more. We set the proportion (E) of protein-altering mutations in risk genes based on point estimate of enrichment in cases compared to expectation (E = (M1–M2)/M1, where M1 and M2 are the observed and expected count of protein-altering *de novo* mutations per trio, respectively). We then simulated the likelihood function as follows: First, we randomly selected G risk genes from the HBE gene set. Next, we simulated the number of contributing protein-altering mutations in risk genes, i.e., C, by sampling once from Binomial(K,E) distribution. Then, we simulated C contributing protein-altering mutations in G risk genes and K-C non-contributing protein-altering mutations in the complete HBE gene set, using each gene's protein-altering mutability score as probability weights. We performed 20,000 simulations for G from 2 to 100, and calculated the likelihood function L(G) as the proportion of simulations in which the number of genes with two protein-altering *de novo* mutations equals to R1 and the number of genes with three or more protein-altering *de novo* mutations equals to R2. We then estimated the number of risk genes using the maximum likelihood estimate (MLE). Based on the likelihood function, we calculated the Fisher information and constructed the confidence interval based on the MLE and estimated Fisher information using the following equation

$$\mathrm{MLE} \pm 1.96 \times \left(\frac{1}{\sqrt{\text{Fisher Information}}} \right)$$

In Situ Hybridization

Mouse brains and embryos were fixed in 4% paraformaldehyde by overnight immersion and sectioned (10-15 μm, cryostat sections for digoxigenin [DIG] probes). Antisense RNA probes corresponding to murine Ptch1, Smarcc1 and Trim71 (approx. 200bp for DIG-labeled probes respectively) were synthesized to detect Ptch1, Smarcc1 and Trim71 transcripts in murine tissue, using methods previously described (Duncan et al., 1994; Petersen et al., 2002; Schaeren-Wiemers and Gerfin-Moser, 1993).

DATA AND SOFTWARE AVAILABILITY

The sequencing data for congenital hydrocephalus case-parent trios reported in this manuscript have been deposited in the NCBI database of Genotypes and Phenotypes (dbGaP). The accession number for the data reported in this paper is dbGaP: phs000744.

Neuron, Volume *99*

Supplemental Information

De Novo Mutation in Genes Regulating Neural Stem Cell Fate in Human Congenital Hydrocephalus

Charuta Gavankar Furey, Jungmin Choi, Sheng Chih Jin, Xue Zeng, Andrew T. Timberlake, Carol Nelson-Williams, M. Shahid Mansuri, Qiongshi Lu, Daniel Duran, Shreyas Panchagnula, August Allocco, Jason K. Karimy, Arjun Khanna, Jonathan R. Gaillard, Tyrone DeSpenza, Prince Antwi, Erin Loring, William E. Butler, Edward R. Smith, Benjamin C. Warf, Jennifer M. Strahle, David D. Limbrick, Phillip B. Storm, Gregory Heuer, Eric M. Jackson, Bermans J. Iskandar, James M. Johnston, Irina Tikhonova, Christopher Castaldi, Francesc López-Giráldez, Robert D. Bjornson, James R. Knight, Kaya Bilguvar, Shrikant Mane, Seth L. Alper, Shozeb Haider, Bulent Guclu, Yasar Bayri, Yener Sahin, Michael L.J. Apuzzo, Charles C. Duncan, Michael L. DiLuna, Murat Günel, Richard P. Lifton, and Kristopher T. Kahle

Supplemental Figures

Figure S1 – Principal component analysis (related to Table 2, Figure 4). (A) Principal-component analysis of our hydrocephalus cohort of 440 individuals (+) clustered along with HapMap subjects (o). (B) Principal-component analysis of 177 probands with congenital hydrocephalus clustered along with HapMap subjects. Results identify 162 probands (+) that cluster with HapMap Non-Finnish, European subjects (o).

A

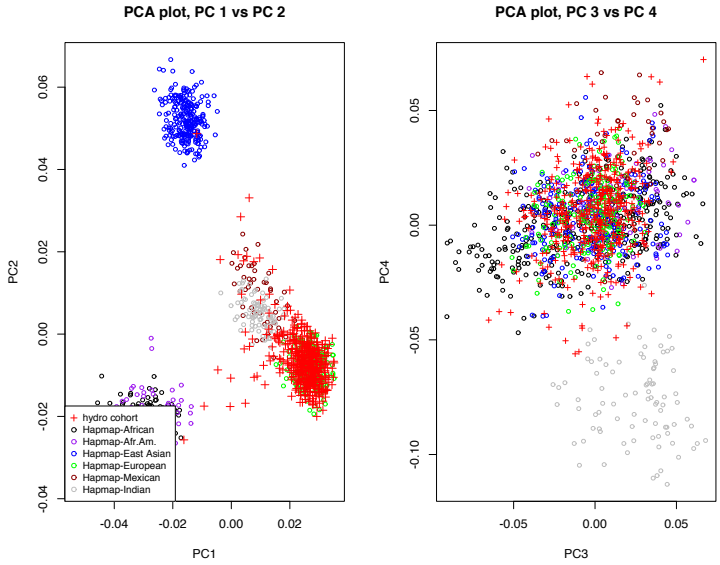

B

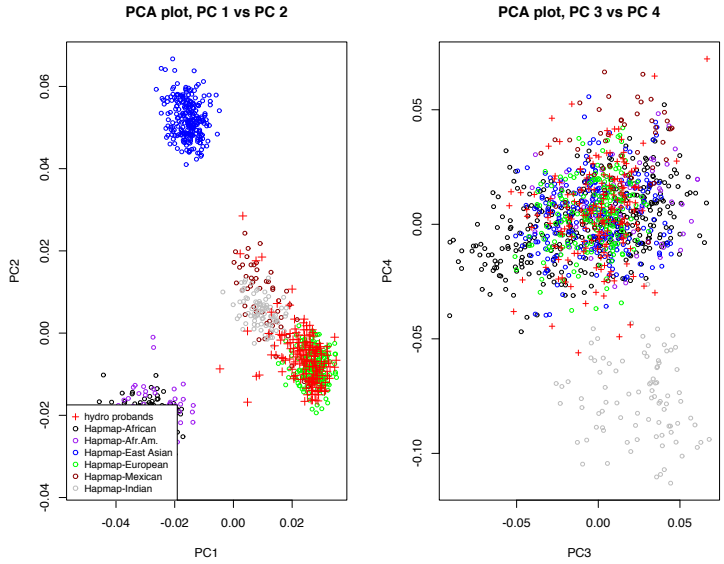

Figure S2 – *De novo* mutation rates closely approximate a Poisson distribution in cases and controls (related to Tables 1-2, Figure 4). Observed number of *de novo* mutations per case-parent trio (bars) compared to expected (line) from the Poisson distribution in CH case (red) and healthy autism sibling control (blue) cohorts; 'p' denotes the chi-squared p-value.

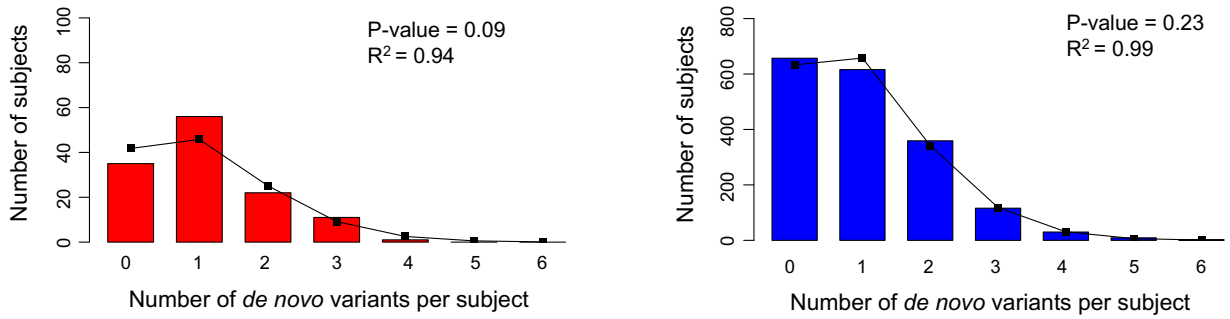

Figure S3 – Structural modeling of *TRIM71* mutation impact (related to Figure 1). (A) Homology model of TRIM71 (residues 577-868) based on the crystal structure of the Brat-NHL domain. TRIM71 belongs to the NHL superfamily exhibiting structural conservation of the hexa-NHL repeat. R608 and R796 are shown as cyan sticks. (B) Surface representation of TRIM71 (white surface with R608 and R796 in blue) with bound 14-nucleotide RNA (orange backbone with nucleotides as green sticks). (C) The positively charged TRIM71 guanidinium side chain of p.Arg796 interacts with the sugar-phosphate backbone of its target RNA, possibly stabilizing the spatial orientation of the nucleic acid. The imidazole ring of the missense mutant histidine (ΔΔG = 2.0 Kcal/mol) is unable to retain these interactions. (D) The R608 guanidinium side chain makes hydrogen bonds with a uracil base of its target RNA. The p.Arg608His mutation (ΔΔG = 1.6 Kcal/mol) results in the loss of these hydrogen bonds. (E) TRIM71 (cyan surface) and TRIM71 residues (yellow surface) within 5Å of bound RNA (cpk sticks) with spatial positions of p.Arg608 and p.Arg796 labeled. (F) Lateral and (G) Superior view of RNA (green) interacting with TRIM71. The surface of TRIM71 is colored based on an electrostatic surface representation. The part of the RNA interacting interface is positively charged (blue). (H) Eight nucleotides that interact with TRIM71 have been illustrated by surface representation and the color highlights the surface charge pattern. It is worth noting the complementary electrostatic charge pattern at the interface of RNA (red) and TRIM71 (blue).

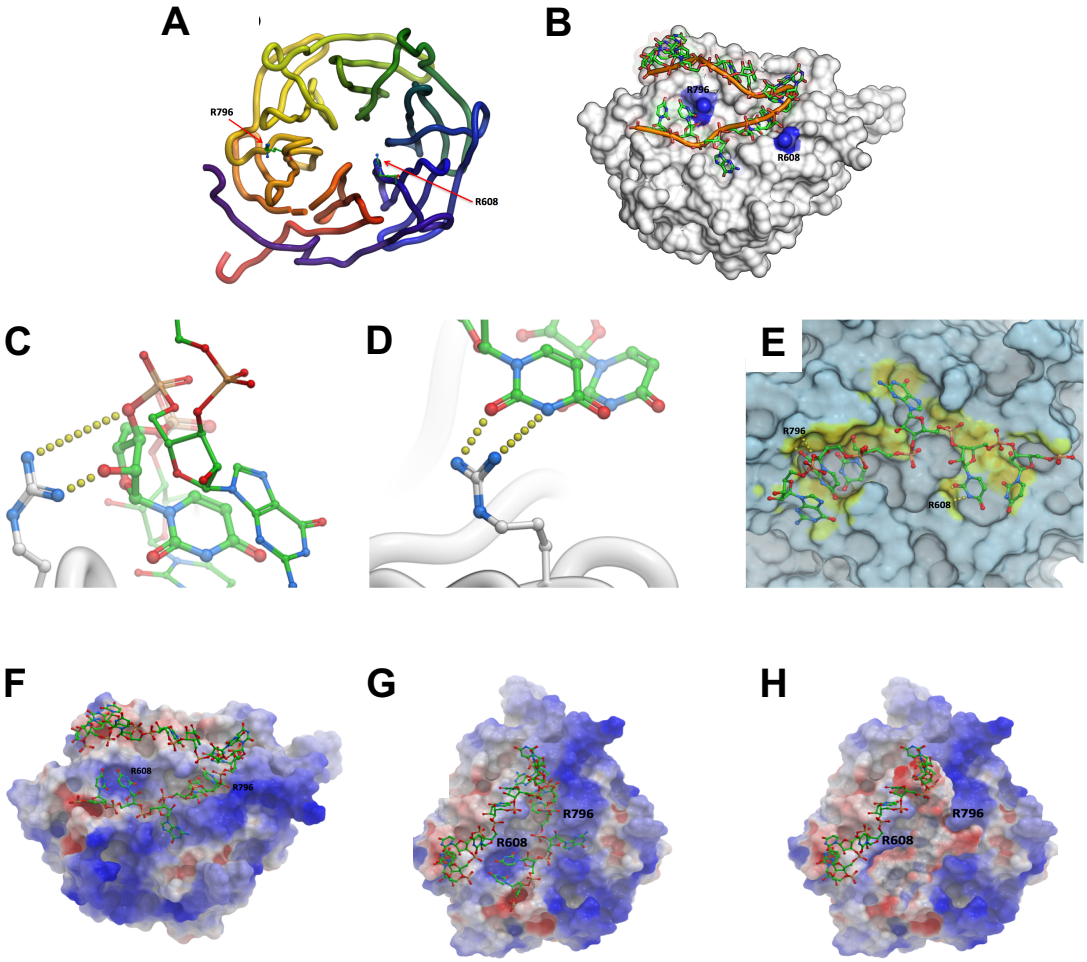

Figure S4 – *In situ* hybridization staining of wild-type mouse embryos for Trim71, Smarcc1, and Ptch1 in the embryonic day 12.5 (E12.5, 2.5x) and adult mouse brain (10x magnification) demonstrates specific expression in the ciliated neuroepithelium lining the neural tube and ventricular zone in the developing brain (related to Figures 1-3).

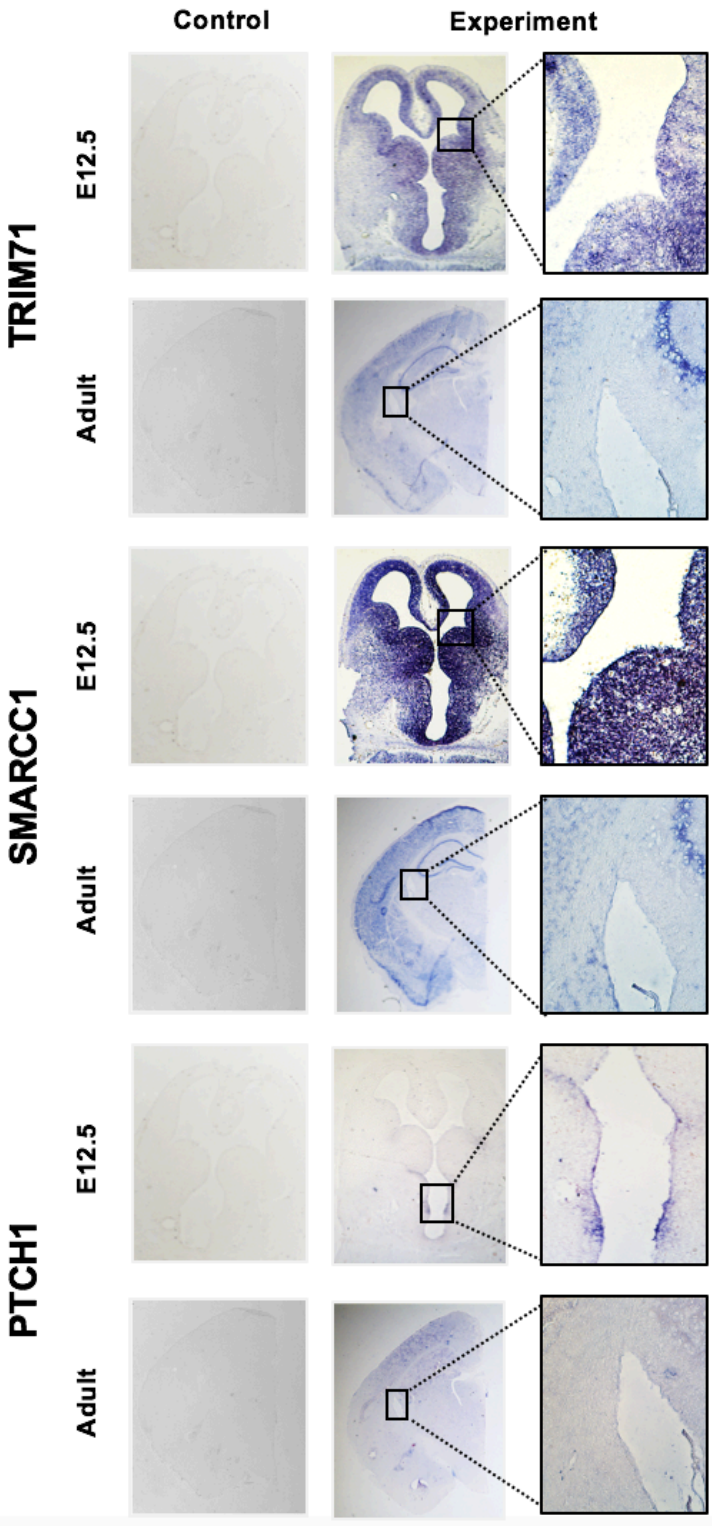

Figure S5 – Pedigrees and Sanger sequence chromatograms for three families carrying *de novo* mutations in *LIN41/TRIM71* (related to Figure 1).

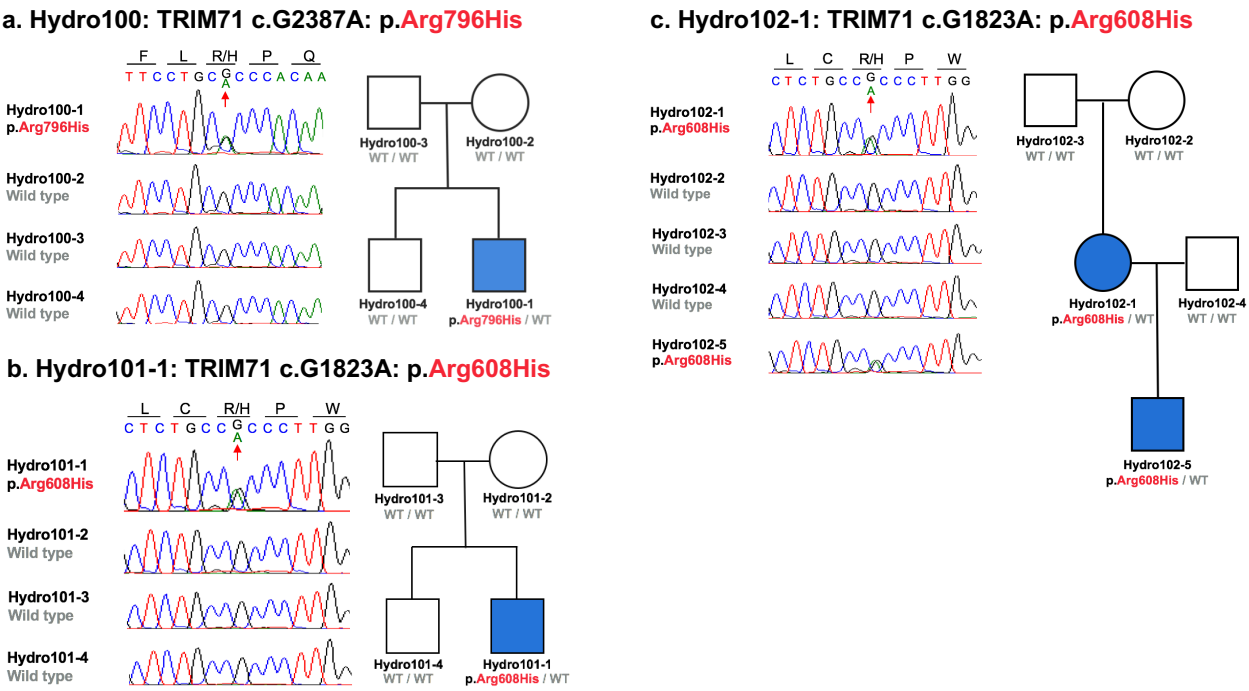

Figure S6 – Pedigrees and Sanger sequence chromatograms for three families carrying damaging mutations in *SMARCC1* (related to Figure 2).

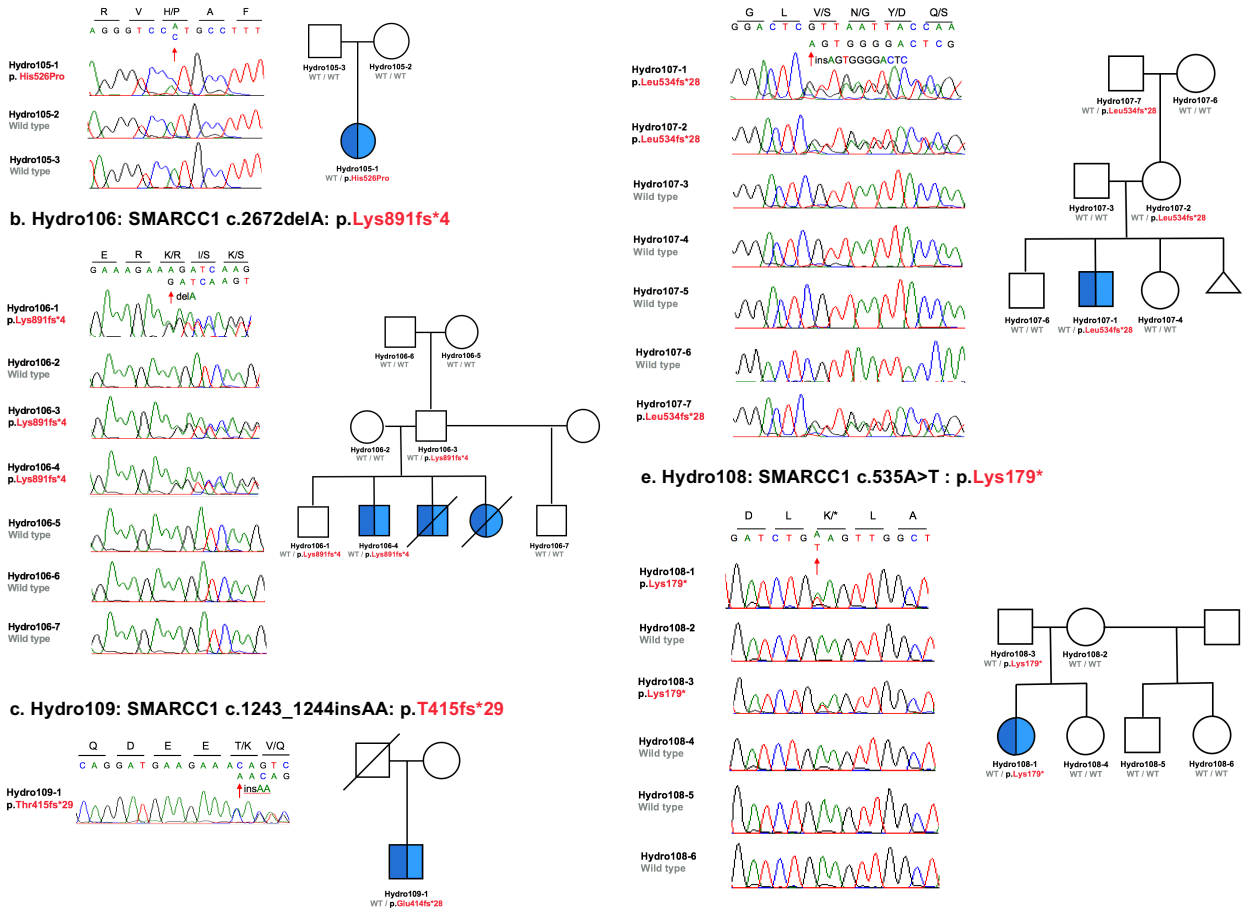

Figure S7 – Pedigrees and Sanger sequence chromatograms for three families carrying loss-of-function mutations in *PTCH1* (related to Figure 3).

a. Hydro103: PTCH1 c.456_457delGT: p.Met152fs*1

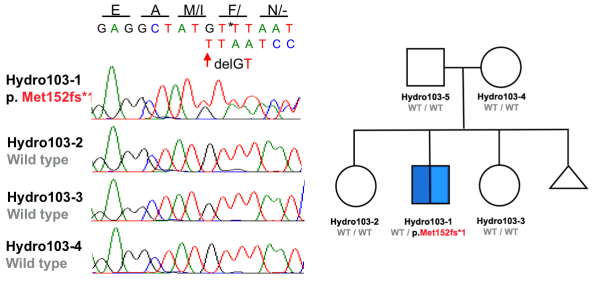

b. Hydro104: PTCH1 c.1503+3T<C

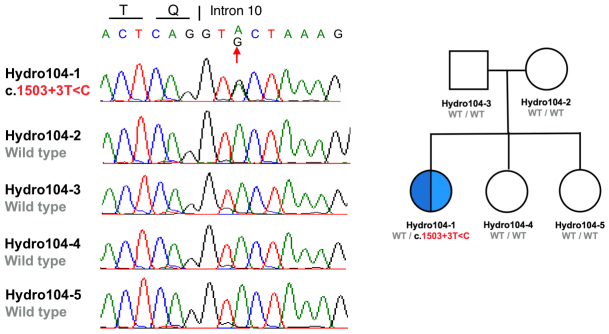

c. HydroFam100: PTCH1 c.1991_1997delTCCGCAC: p.Leu664fs*12

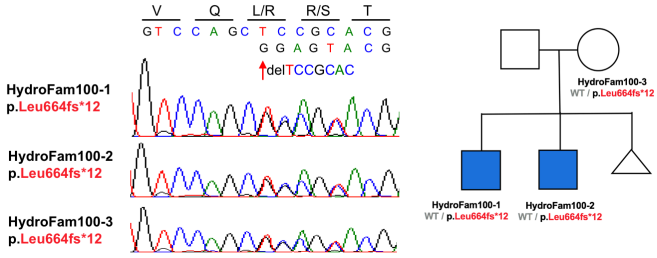

Figure S8 – Estimation of the number of genes contributing to congenital hydrocephalus via *de novo* mutations (related to Tables 1-2, Figure 4). Monte Carlo simulation was performed based on observed protein-altering *de novo* mutations in genes highly expressed in the developing mouse brain using 20,000 iterations. This likelihood-based approach assumes identical penetrance of all protein-altering *de novo* mutations in all risk genes (for details, see Methods). We estimate that the number of risk genes via *de novo* events is ~8 (95% confidence interval: [2.52, 13.48]).

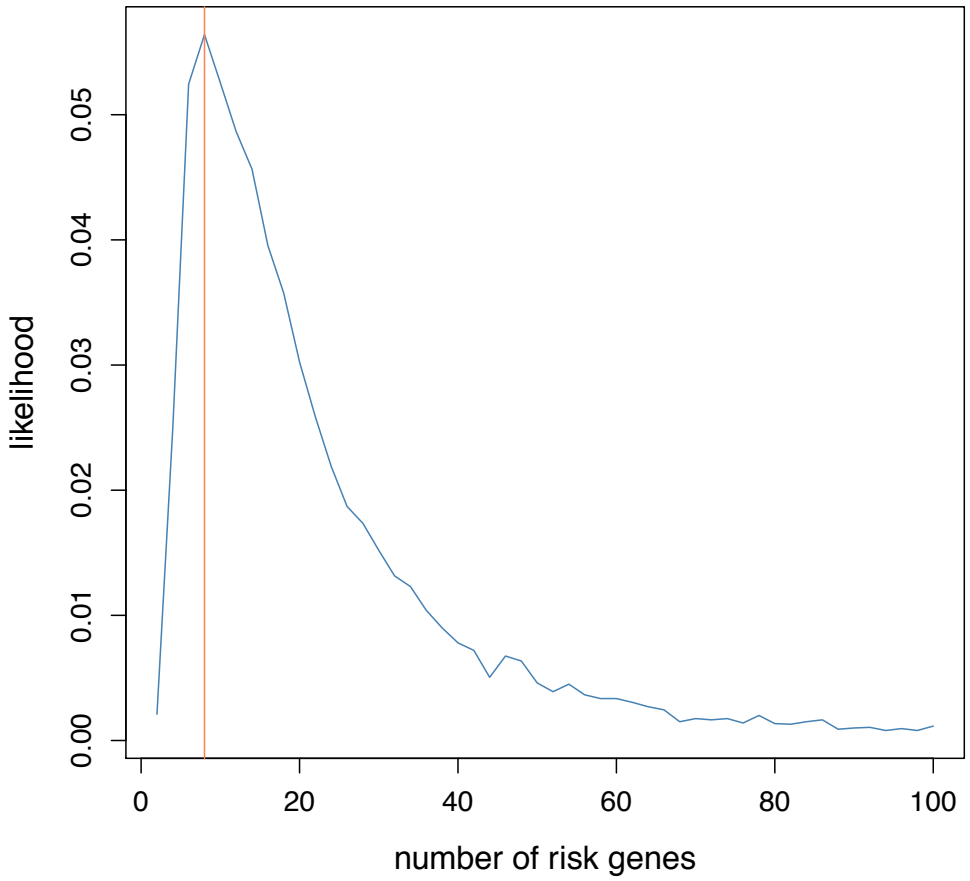

Figure S9 – Saturation analysis for detecting risk genes with more than one protein-altering *de novo* mutation (related to Tables 1-2, Figure 4). The number of trios (x-axis) and the number of risk genes with more than one protein-altering *de novo* mutation (y-axis) are specified. The expected number of risk genes was determined by the maximum likelihood approach to be 8. In each iteration of the simulation, the total number of protein-altering mutations in risk genes was determined based on the point estimate of enrichment in cases compared to expectation (= N×[(M1-M2)/M1], where N is the number of trios and M_1 and M_2 are the observed and expected count of protein-altering *de novo* mutations per trio, respectively). We then randomly distributed this amount across eight randomly-selected risk genes and calculated how many of these eight genes have > 1 protein-altering *de novo* events. 10,000 iterations were performed to estimate the number of risk genes with more than 1 protein-altering *de novo* mutation, taking into account the protein-altering *de novo* mutation probability. Whole exome sequencing of 500 and 1,000 trios will yield 6.4 and 7.6 risk genes, reaching respective saturations for all risk genes of 80% and 95%.

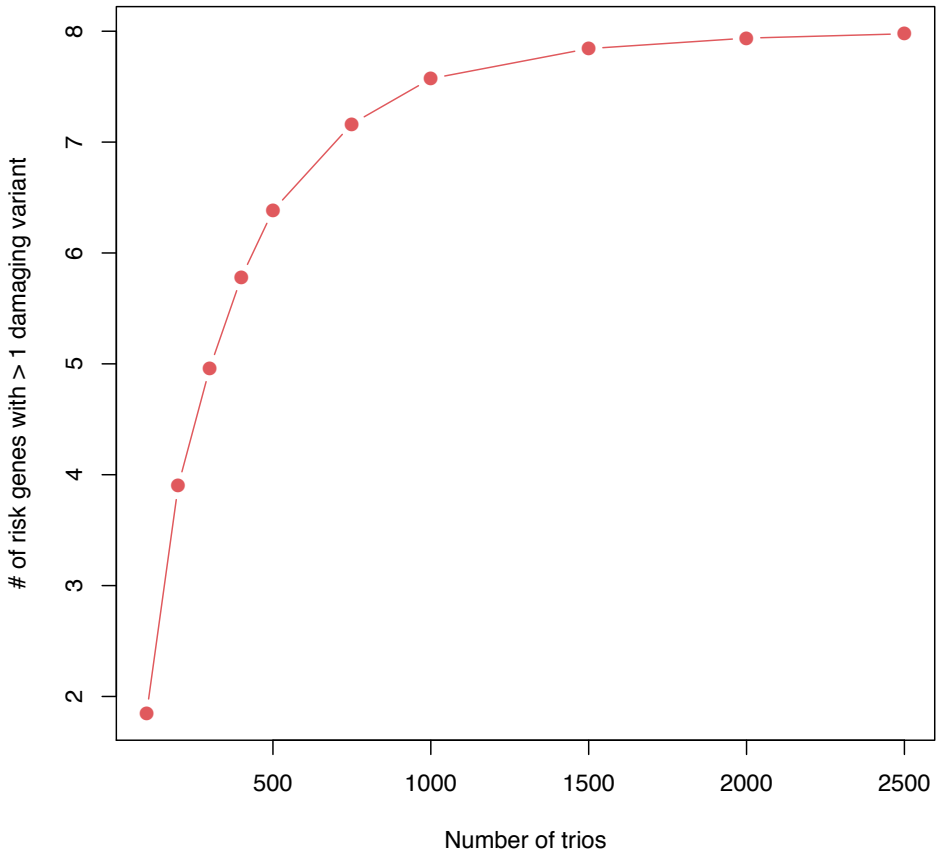

Supplemental Tables

Table S1 – Number of studied congenital hydrocephalus cases and controls (related to Tables 1-2).

Category	N
# of unrelated congenital hydrocephalus probands	177
# of case-parent trios	125
# of singleton cases	47
# of familial forms	5
# of control case-parent trios	1,789

N: Number of case-parent trios, singleton cases, and familial forms (defined as greater than one patient in nuclear family affected by congenital, primary hydrocephalus)

Table S2 – Demographic and summary sequencing statistics for the congenital hydrocephalus (CH) and control cohorts (related to Tables 1-2).

Category	CH Cases (xGen IDT; N = 440)	Autism Cohort Sibling Controls (Roche V2; N = 5,367)
Sample Size	177	1,789
Gender		
Male	90 (50.8%)	840 (47.0%)
Female	87 (49.2%)	949 (53.0%)
Ethnicity		
European	162 (91.5%)	1,408 (78.7%)
Mexican	11 (6.2%)	79 (4.4%)
African American	1 (0.56%)	41 (2.3%)
East Asian	1 (0.56%)	87 (4.9%)
South Asian	2 (1.0%)	125 (7.0%)
Other	0 (0.0%)	49 (2.7%)
Sequencing statistics		
Read length (bp)	99	50-94
# of reads per sample (M)	50.99	99.7
Median coverage at each targeted base (X)	49.91	67
Mean coverage at each targeted base (X)	54.33	79.1
% of all reads that map to target	57.64%	57.6%
% of all bases that map to target	43.81%	49.0%
% of targeted bases read at least 8x	95.90%	94.6%
% of targeted bases read at least 10x	95.28%	93.4%
% of targeted bases read at least 15x	92.70%	89.9%
% Mean error rate	0.29%	0.4%

The number of samples is shown in each category with the corresponding percentage in parenthesis. Ethnicity is determined by principal component analysis compared to HapMap samples using EIGENSTRAT (see **Methods**). All hydrocephalus cohort samples were sequenced using the xGen IDT capture reagent. 8X, 10X and 15X target base coverage was comparable across platforms.

Table S3 – Observed and expected *de novo* mutation rates in 1,789 healthy autism controls for variant classes (related to Table 1).

	Observed		Expected		Enrichment	p
	n	Rate	n	Rate		
Control, Healthy Autism Sibling Cohort						
All	1830	1.02	1949.9	1.09	0.94	1.00
Synonymous	484	0.27	549.6	0.31	0.88	1.00
Missense	974	0.54	993.3	0.56	0.98	0.81
D-Mis	222	0.12	232.8	0.13	0.95	0.77
LOF	150	0.08	174.3	0.10	0.86	0.97
Protein-Altering	1346	0.75	1400.3	0.78	0.96	0.93
Damaging	372	0.21	407.1	0.23	0.91	0.96

n: the number of *de novo* mutations; Rate: the number of *de novo* mutations per individual; Enrichment: ratio of observed to expected numbers of mutations; Missense: tolerated missense mutations as predicted by MetaSVM; D-Mis: damaging missense mutations as predicted by MetaSVM; LOF: loss-of-function denotes premature termination, frameshift or splice site mutation; Damaging: D-Mis and loss-of-function mutations

Table S4 – Genes with multiple *de novo* mutations in 125 congenital hydrocephalus case-parent trios (observed vs. expected; related to Table 1). Observed and expected numbers of genes with greater than 1 *de novo* mutation in each variant category using a Monte Carlo simulation

	Observed	Expected	Enrichment	P-value
Total	5	0.948	5.27	**2.4×10^{-3}**
Synonymous	0	0.053	0.00	1.00
Missense	3	0.407	7.37	**7.4×10^{-3}**
Damaging (LOF + D-Mis)	3	0.074	40.81	**5.5×10^{-5}**
D-Missense	1	0.028	35.46	**0.028**
Loss of Function (LOF)	1	0.013	76.37	**0.013**

N: Number of case-parent trios, singleton cases, and familial forms (defined as greater than one patient in a nuclear family affected by congenital, primary hydrocephalus)

Table S5 – High brain expressed genes (Top Quartile) with multiple *de novo* mutations in 125 congenital hydrocephalus case-parent trios (observed vs. expected; related to Table 1). Observed and expected numbers of high brain expressed genes (top 25% in the developing mouse brain) with greater than 1 *de novo* mutation in each variant category

	Observed	Expected	Enrichment	P-value
Total	4	0.26	15.5	**1.1×10^{-4}**
Synonymous	0	0.01	0	1
Missense	2	0.11	18.4	**5.4×10^{-3}**
Damaging (LOF + D-Mis)	3	0.02	151.7	**1.0×10^{-6}**
D-Missense	1	0.008	132.6	**7.5×10^{-3}**
Loss of Function (LOF)	1	0.004	279.5	**3.6×10^{-3}**

N: Number of case-parent trios, singleton cases, and familial forms (defined as greater than one patient in a nuclear family affected by congenital, primary hydrocephalus)

Table S6 – *De novo* mutations in *TRIM71/LIN-41* (related to Figure 1 and Table 2).

Patient ID	Gene	Mutation	AA Change	Chr	Pos	Ref	Alt	gnom AD	ExAC	pLI	Poly phen	Meta SVM	CADD	MPC	Substitutions among 46 species
Hydro 100-1	*TRIM71 / LIN41*	*De Novo* Missense	p.Arg796 His	3	32933083	G	A	Novel	Novel	0.99	D	T	26.3	2.3	0
Hydro 101-1	*TRIM71 / LIN41*	*De Novo* Missense	p.Arg608 His	3	32932519	G	A	Novel	Novel	0.99	D	T	32	2.3	0
Hydro 102-1	*TRIM71 / LIN41*	*De Novo* Missense	p.Arg608 His	3	32932519	G	A	Novel	Novel	0.99	D	T	32	2.3	0
Hydro 102-5	*TRIM71 / LIN41*	Transmitted Missense	p.Arg608 His	3	32932519	G	A	Novel	Novel	0.99	D	T	32	2.3	0

Table S7 – *De novo* and damaging transmitted mutations in *SMARCC1/BAF155* (related to Figure 2 and Table 2).

Patient ID	Gene	Mutation	Inheritance	AA Change	Chr	Pos	Ref	Alt	gnom AD	ExAC	pLI	Poly phen	Meta SVM	CADD	MPC	Substitutions among 46 species
Hydro 105-1	*SMARCC1 / BAF155*	D-Mis Mutation	*De Novo*	p.His526Pro	3	47718267	T	G	Novel	Novel	1	D	D	28.9	2.6	0
Hydro 106-3	*SMARCC1 / BAF155*	Frameshift Deletion	*De Novo*[1]	p.Lys891fs*4	3	47663806	T	-	Novel	Novel	1	.	.	.	.	0
Hydro 107-1	*SMARCC1 / BAF155*	Frameshift Insertion	Transmitted	p.Leu534fs*28	3	47718254	-	GAG TCC CCA CT	Novel	Novel	1	.	.	.	.	3
Hydro 108-1	*SMARCC1 / BAF155*	Stop Gain Mutation	Transmitted	p.Lys179*	3	47777565	T	A	Novel	Novel	1	.	.	37	.	0
Hydro 109-1	*SMARCC1 / BAF155*	Frameshift Insertion	Unknown[2]	p.Thr415fs*29	3	47730896	-	TT	Novel	Novel	1	.	.	.	.	0

[1] This *de novo* mutation was transmitted from an unaffected father (Hydro106-3) to an affected proband (Hydro106-1).
[2] This proband's biological father is deceased and biological mother is estranged.

Table S8 – *De novo* and damaging transmitted mutations in *PTCH1* (related to Figure 3 and Table 2).

Patient ID	Gene	Mutation	Inheritance	AA Change	Chr	Pos	Ref	Alt	gnom AD	ExAC	pLI	Substitutions among 46 species
Hydro 103-1	*PTCH1*	Frameshift Deletion	*De Novo*	p.Met152fs*1	9	98248093	AAC	A	Novel	Novel	1	.
Hydro 104-1	*PTCH1*	Splice Donor	*De Novo*	c.1503+3T>C	9	98239826	A	G	Novel	Novel	1	0
HydroFam 100-1	*PTCH1*	Frameshift Deletion	Transmitted	p.Leu664fs*12	9	98231286	GTGC GGA	-	Novel	Novel	1	.

Table S9 – *De novo* mutations in *PLOD2* (related to Figure 4 and Table 2).

Patient ID	Gene	Mutation	AA Change	Chr	Pos	Ref	Alt	gnomAD	ExAC	Poly phen	Meta SVM	CAD D	Substitutions among 46 species
Hydro 229-1	*PLOD2*	D-Mis	p.Arg473Gln	3	145796985	C	T	$3.26x10^{-5}$	$3.78x10^{-5}$	D	D	25	1
Hydro 245-1	*PLOD2*	D-Mis	p.Thr643Met	3	145789068	G	A	$2.85x10^{-5}$	$2.84x10^{-5}$	D	D	28	1

Table S10 – *De novo* enrichment analysis for neural tube defect genes in cases and controls (related to Table 1).

	Observed		Expected		Enrichment	*p*
	N	Rate	N	Rate		
CH Cases (N=125) ***Neural tube defect genes (N = 184)***						
All	10	0.080	2	0.016	4.96	**5.0×10^{-5}**
Syn	1	0.008	0.6	0.005	1.69	0.45
Missense	6	0.048	1.3	0.010	4.74	**2.0×10^{-3}**
D-Mis	1	0.008	0.3	0.002	3.27	0.26
LOF	3	0.024	0.2	0.002	18.7	**6.1×10^{-4}**
Protein-Altering	9	0.072	1.4	0.011	6.32	**1.9×10^{-5}**
Damaging	4	0.032	0.5	0.004	8.58	**1.4×10^{-3}**
Controls (N=1,789) ***Neural tube defect genes (N = 184)***						
All	26	0.015	27.8	0.016	0.94	0.66
Syn	7	0.004	8.1	0.005	0.87	0.69
Missense	18	0.010	17.5	0.010	1.03	0.48
D-Mis	6	0.003	4.3	0.002	1.39	0.27
LOF	1	0.001	2.3	0.002	0.44	0.90
Protein-Altering	19	0.011	19.8	0.011	0.96	0.60
Damaging	7	0.004	6.6	0.004	1.06	0.49

Table S11 – *De novo* copy number variants in 125 case-parent trios with congenital hydrocephalus (related to Table 1).

Patient ID	Chr	Start	End	Length	Alteration	SQ score	# Exons	Genes in the region	1000G frequency
Hydro 154-1	5	170814836	171100000	285164	Duplication	96	15	*FGF18, NPM1*	Novel
Hydro 154-1	5	172068277	172342131	273854	Duplication	96	15	*DUSP1, ERGIC1, LOC101928093, NEURL1B*	0.002
Hydro 134-1	6	170591818	170713790	121972	Deletion	95	18	*DLL1, FAM120B*	Novel
Hydro 269-1	7	154735732	155604899	869167	Duplication	95	54	*CNPY1, EN2, HTR5A, INSIG1, PAXIP1, RBM33, SHH*	Novel
Hydro 131-1	7	155599390	155755985	156595	Duplication	76	3	*LOC389602, SHH*	Novel
Hydro 198-1	11	61731700	61734947	3247	Duplication	95	4	*FTH1*	Novel